JOURNAL OF PETROLOGY | VOLUME 50 | NUMBER 8 | PAGES 1505–1531 | 2009 | doi:10.1093/petrology/egp039

Modeling the Magnitudes and Directions of Regional Metamorphic Fluid Flow in Collisional Orogens

T. LYUBETSKAYA* AND J. J. AGUE

DEPARTMENT OF GEOLOGY AND GEOPHYSICS, YALE UNIVERSITY, PO BOX 208109, NEW HAVEN, CT 06520-8109, USA

RECEIVED OCTOBER 12, 2008; ACCEPTED MAY 25, 2009
ADVANCE ACCESS PUBLICATION JULY 7, 2009

We present two-dimensional numerical models that simulate fluid flow in an orogenic overthrust setting in the absence of magmatism. The modeling is intended to test hypotheses regarding the direction of regional fluid flow in the middle and deep crust, including upward, convective, sub-horizontal, up-temperature, and down-temperature flow regimes. Several geological factors that have received relatively little attention in previous numerical models of regional metamorphic fluid flow are considered: (1) retrograde hydration metamorphic reactions; (2) anisotropy and spatial heterogeneity in crustal permeability structure; (3) temporal evolution of permeability as a result of porosity production and consumption during metamorphic reactions; (4) heat of metamorphic reactions. Our results suggest that the typical fluid flow pattern in overthrust settings is towards the surface, in the direction of decreasing temperature. The flow is mainly driven by metamorphic dehydration reactions; the integrated fluxes in the deep crust below 20 km are of the order of 10^3 m^3/m^2 over 30 Myr for a background permeability of 10^{-19} m^2. At higher crustal permeability, the buoyancy flux generally exceeds the metamorphic flux and large-scale fluid circulation becomes possible. Transient upward flow in the up-temperature direction is observed during the first 1–3 Myr of the model evolution within the thrust core that undergoes retrograde hydration; this flow is the result of the initially inverted geotherm in the thickened crustal section. Downward fluid infiltration caused by metamorphic hydration may occur in the flanks of the model orogen, but the integrated fluxes in these areas are only ~10 m^3/m^2. Hydration-driven downward flow may also develop in the core of the orogen at late stages of exhumation. Low-permeability layers lead to sub-horizontal (but down-temperature) flow over distances corresponding to the lateral dimensions of such layers. Heterogeneities in permeability structure, as well as porosity–permeability variations produced by metamorphic reactions, result in focusing of fluid flow and locally elevated fluid fluxes (up to 10^4 m^3/m^2). These fluxes are large enough to produce significant chemical and isotopic metasomatism, but are not sufficient to significantly affect the temperature distribution in the model orogen. However, metamorphic hydration and dehydration reactions are found to exert considerable control on the regional thermal structure. We conclude that convective, downward, or up-temperature fluid flow is probably very limited during amagmatic prograde metamorphism of the middle and lower crust, even in the presence of permeability anisotropy, high-permeability channels, or low-permeability barriers.

KEY WORDS: *fluid flow; fluid flux; hydration; metamorphism; orogen*

INTRODUCTION

The character and regime of fluid flow in the continental crust is a central issue of metamorphic petrology. Whereas the hydrological behavior of the upper crust is relatively well understood (e.g. Garven, 1995), fluid flow patterns in the deep crust are subject to considerable debate. High fluid pressures and low permeabilities have been proposed to lead to pervasive flow towards the surface via a crack opening mechanism (Walther & Orville, 1982; Walder & Nur, 1984). On the other hand, high fluid pressures in the deep crust could possibly produce deformation (hydrofracture) and enhanced permeability, leading to fluid circulation in large-scale convective cells (Etheridge *et al.*, 1983, 1984). The large-scale lateral flow of fluid has been hypothesized to result from anisotropy in permeability structure (Manning & Ingebritsen, 1999), or spatial

*Corresponding author. E-mail: tanya.lyubetskaya@yale.edu

variations in crustal permeability (Oliver, 1996) in the middle and deep crust.

Deep crustal fluid flow models are not easy to evaluate, as the available data on fluid fluxes come from inverse geochemical and petrological modeling of field and laboratory observations of metamorphic rocks. The chemical and isotopic compositions of minerals are used to infer depths, temperatures and pressures of metamorphism, to estimate the time-integrated fluid fluxes and the directions of fluid flow. This inverse approach may sometimes yield contradictory results. In particular, records of fluid–rock interactions in metasedimentary rocks in New England demonstrate the prograde loss of CO_2, which has been interpreted as an indication of flow of fluid in the direction of increasing temperature (Baumgartner & Ferry, 1991; Ferry, 1992). Pervasive regional up-temperature fluid flow in many metamorphic orogens has also been suggested based on oxygen isotope data (Dipple & Ferry, 1992). Other studies (Ague & Rye, 1999; Evans & Bickle, 1999) have argued that substantial prograde loss of CO_2 from metacarbonate rocks may occur without the requirement of up-temperature flow. Recent three-dimensional (3-D) inversions of reaction progress and isotopic data suggest that metamorphic fluid flow may be highly variable locally, with both up-temperature and down-temperature regimes, but is predominantly upward on a large scale (Wing & Ferry, 2002, 2007). These conflicting conclusions reflect the potential non-uniqueness of inverse modeling of petrological observations, which represent an integrated response to many physical and chemical processes that occur in crustal settings over geological time.

Forward numerical modeling constitutes a useful supplementary tool to the inverse geochemical and petrological calculations: it provides a temporal picture of evolving temperature, pressure and fluid flow in a large-scale metamorphic setting, and helps to illuminate the relationships between many parameters affecting crustal fluid flow.

Classic early numerical models of regional metamorphism focused on thermal evolution of one-dimensional (1-D) sections of thickened crust; they evaluated the timescales of thermal relaxation and constructed model *PTt*-paths (e.g. England & Thompson, 1984), and estimated metamorphic fluid fluxes (e.g. Peacock, 1989). Later works presented two-dimensional (2-D) models that attempted to determine the patterns of fluid flow in upper crustal orogenic settings (Forster & Evans, 1991; Garven & Freeze, 1984*a*, 1984*b*), and in contact metamorphism around shallow intrusions (Hanson & Barton, 1989; Hanson, 1992; Cui *et al.*, 2002). The study by Hanson (1997) presented a 2-D crustal-scale model of fluid flow during continental collision, with thermally driven metamorphic devolatilization reactions. The results of this modeling suggest that the direction of fluid flow in regional metamorphism is predominantly upward, and that the widespread flow of fluid towards higher temperature regions at depth is unlikely. This model, however, did not take into account crustal anisotropy or spatial heterogeneities in permeability, which may divert fluid flow from upward motion (e.g. Manning & Ingebritsen, 1999). Metamorphic hydration reactions represent another possible mechanism that may lead to sideways or downward flow, as suggested by the field observations of Yakovlev (1993) and Stober & Bucher (2004). Metamorphic hydration, however, has not been considered in numerical simulations of large-scale fluid flow.

A new class of crustal fluid flow models has been developed over the last 10–15 years. In these two-phase models, fluid moves through a deformable matrix with porosity and permeability that continuously evolve in response to changes in fluid pressure (e.g. Vasilyev *et al.*, 1998; Connolly & Podladchikov, 1998). Rock deformation accompanying fluid flow is expected to be especially important for compacting sedimentary basins and for deep crustal high-temperature and high-pressure conditions. One important aspect of the two-phase models is their prediction of fluid flow via episodic waves of fluid-filled porosity (e.g. Connolly & Podladchikov, 2000). The two-phase models, however, are strongly dependent on the rheological properties of crustal rocks, which are not tightly constrained. Most studies in this area thus focus primarily on exploring different rheological laws and porosity–permeability behavior in specific geological settings, usually sedimentary basins (e.g. Suetnova & Vasseur, 2000; Morency *et al.*, 2007).

This study presents 2-D models of crustal fluid flow in response to thermal perturbation resulting from overthrusting, metamorphic hydration and dehydration reactions, and permeability variations. The models do not account for the deformation of the rock matrix and the evolution of porosity and permeability in response to the changes in fluid pressure, except for the case of hydrofracturing. This approach is justified in part by the fact that rock deformation is strongest early in the orogen history during crustal collision and overthrusting, whereas our models focus on the post-collisional evolution. They use permeability values based on the empirical depth-dependent permeability curve of Manning & Ingebritsen (1999), which is expected to represent the temporal and spatial average of permeability–porosity fluctuations in response to small-scale rock deformation. The approach used herein, characterized by a non-deformable rock matrix and interconnected porosity, represents the most favorable environment for the unobstructed flow of fluid in any direction. Thus, it is critical to emphasize that our simulations explore the limiting case for the distribution and magnitudes of convective, downward, and up-temperature fluid flow in deep crustal systems that lack magmatism. The models are not intended to represent any

specific metamorphic system, but are constructed to study the interplay between various parameters of metamorphism, and to test the existing hypotheses on the directions of fluid flow.

The simulations incorporate several phenomena that have received relatively little attention in previous simulations of regional metamorphic fluid flow. First, we investigate the effect of hydration reactions on the directions of crustal fluid flow. The capacity of metamorphic hydration reactions to produce downward and up-temperature flow is analyzed as a function of permeability, fluid fluxes, and cooling rates. Second, we incorporate anisotropy and spatial heterogeneity in crustal permeability. In particular, we test several scenarios of spatially variable and anisotropic permeability that are specifically designed to investigate lateral or up-temperature flow. Permeability structures that include narrow fracture zones are used to examine the focusing of the flow and the potential effect of elevated fluid fluxes on the thermal structure of a metamorphic terrane. Third, fluid flow in response to the temporal evolution of crustal permeability is studied with models that simulate hydrofracturing at elevated fluid pressures, and the production and consumption of porosity in metamorphic reactions. Finally, we include the effect of latent heat of metamorphic reaction into the calculations of the model heat budget. Although Connolly & Thompson (1989) showed that this effect could be non-trivial, the latent heat of reaction is commonly neglected in models of metamorphism. In all cases, we examine the directions and temporal evolution of fluid flow, and evaluate the time-integrated fluid fluxes. In addition, we monitor the temperature field of a model metamorphic terrane over its geological lifetime, and assess the contributions of different heat-transfer agents to the total metamorphic heat budget.

MODEL FORMULATION

The model crustal section is designed to represent a continental collision setting, with horizontal dimension 240 km and vertical dimension 80 km (Fig. 1a). The model geometry is close to that used by Hanson (1997): a thrust sheet 30 km thick was emplaced over a distance of 120 km, and the upper 5 km of the upper plate is elevated above the surface to form the topography. The emplaced section tapers off between 60 km and 120 km from the left boundary.

Energy conservation

The thermal evolution of the model crustal section is described with the conservation of energy equation:

$$\rho_m C_p^m \frac{\partial T}{\partial t} = \nabla \cdot (k_c \nabla T) - C_p^f \nabla \cdot (\mathbf{u} T) - \rho_m C_p^m U \frac{\partial T}{\partial z} + A - \frac{\Delta H_r Q_r}{M_{H_2O}}. \quad (1)$$

The right side of the equation includes major mechanisms of heat transport: thermal conduction, the advection of heat by fluid (second term) and by exhuming rock (third term), radiogenic heating, and latent heat of reaction, respectively (see Table 1 for the list of variables). Mechanical dispersion is neglected in this treatment; thermal conductivity (k_c) is assumed constant within the crust at 2·25 W/m/K in most of our simulations (e.g. England & Thompson, 1984; Hanson, 1997; Jamieson *et al.*, 1998). To test the effect of constant k_c on our models, we ran supplementary simulations in which thermal conductivity was assumed to be temperature-dependent based on relationships suggested by Gerya *et al.* (2002) for a dioritic composition within the crust and an ultramafic composition within the mantle (see Table 2 for a list of the model runs). Despite the noticeable effects of temperature-dependent conductivity on the thermal evolution of the model thrust [see Gerya *et al.* (2002) for discussion], the crustal-scale fluid flow patterns with constant and temperature-dependent k_c are very similar because the major controls on fluid flow are exerted by crustal permeability and the distribution of fluid sinks and sources within the crust.

Radiogenic heat production and mantle heating; initial temperature

The mean surface heat flow in different geological provinces in the continental crust varies roughly in the range of 30–90 mW/m^2 (e.g. Jaupart & Mareschal, 2003). Younger provinces less than 250 Myr old tend to have higher surface heat flow, sometimes exceeding 100 mW/m^2 (Sclater *et al.*, 1981; Pollack *et al.*, 1993). The relative contributions of crust and mantle to the surface heat flow are inferred from geochemical data on the crustal content of heat-producing elements, and seismic velocities in the lower crust (e.g. Rudnick *et al.*, 1998). The radiogenic heat production at the surface of continents is on average 1–3·5 mW/m^3 (e.g. Jaupart & Mareschal, 2003), but it is expected to diminish with depth as a result of decreasing abundances of heat-producing elements (Rudnick & Fountain, 1995). The estimates of the mantle contribution to the heat flow are 20–30 mW/m^2 in old stable regions of continental crust (Sclater *et al.*, 1981; Jaupart & Mareschal, 2003), whereas younger Phanerozoic provinces are generally characterized by higher mantle heat flows, sometimes exceeding 60 mW/m^2 (e.g. Cermak, 1993; Rimi, 1999).

We use a representative surface heat flow value of 65 mW/m^2, and a mantle heat flow component of 45 mW/m^2. The concentration of radiogenic heat-producing elements in the crust is assumed to decay exponentially with depth with the characteristic length scale of 10 km (Fig. 1b). The surface value of radiogenic heat production, 2×10^{-6} W/m^3, is within the range used by England & Thompson (1984) and is slightly less than that

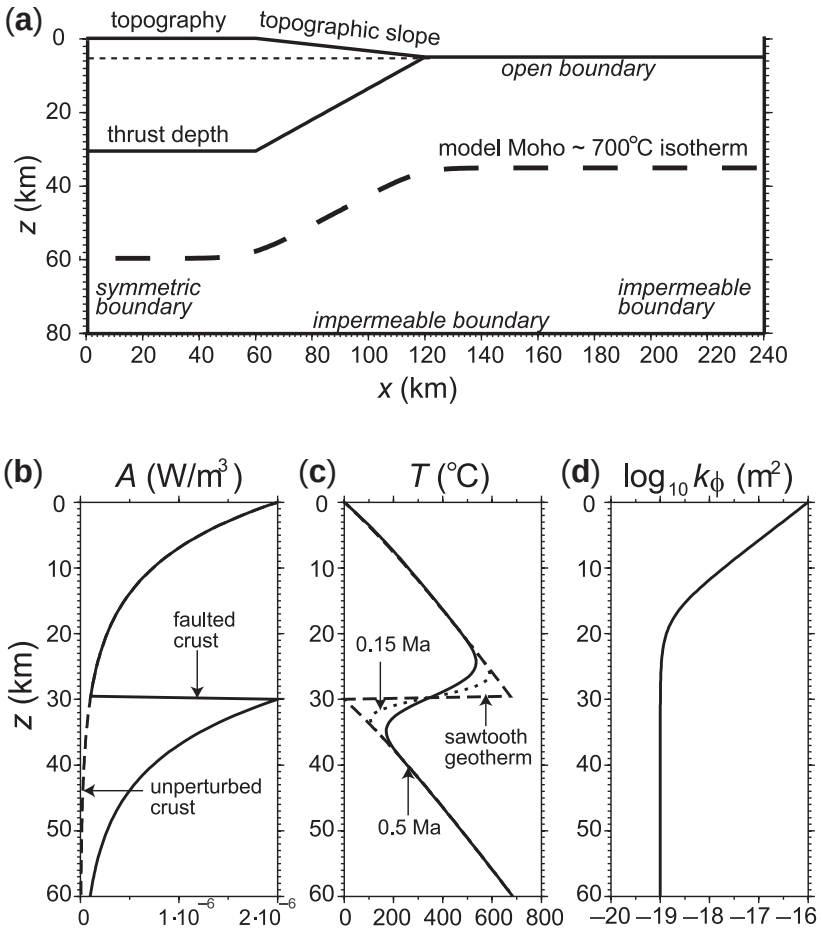

Fig. 1. Geometry of the model and initial conditions. (a) Schematic model geometry. (b) One-dimensional profile of radiogenic heat production within the thrust section (continuous line) and away from the thrust (dashed line). (c) One-dimensional profile of initial temperature distribution within the thrust section: sawtooth geotherm (dashed line), geotherm after 0·15 Myr of conductive relaxation (dotted line), geotherm after 0·5 Myr of conductive relaxation (continuous line). (d) One-dimensional profile of reference crustal permeability structure.

used by Hanson (1997; 3×10^{-6} W/m^3). The latter model, however, did not include radiogenic heating in the upper plate of the thrust section.

The initial thermal structure of the model is calculated based on a steady-state crustal geotherm (Turcotte & Schubert, 2002):

$$T = T_s + \frac{q_m z}{k_c} + \frac{A z_A^2}{k_c}(1 - e^{-z/z_A}). \quad (2)$$

The right boundary is maintained at a steady-state temperature distribution over the entire simulation time. The left boundary is symmetrical, and does not transfer heat in the horizontal dimension; the surface has a constant temperature $T_s = 0$°C. The model Moho (mantle–crust boundary) corresponds to the 700°C isotherm, yielding an unperturbed crustal thickness of ~30 km. In the thrust region, the initial superimposition of two crustal plate geotherms results in a sawtooth geotherm (Fig. 1c). Shi & Wang (1987) suggested, however, that the sawtooth would require unrealistically high convergence rates. Therefore, we allow the initial sawtooth temperature distribution to relax conductively for 0·5 Myr before the simulations start. In addition, we consider a special case of increased convergence rates using a model that starts after only a 0·15 Myr period of conductive relaxation.

An alternative thermal structure was used in a supplementary model intended to test the effect of the thermal regime on the fluid flow (not shown). In this model, a slightly lower surface heat flow, ~60 mW/m^2, is the result of a relatively low mantle heat flow of 35 mW/m^2 and slightly increased radiogenic heating (surface value equal 3×10^{-6} W/m^3). The lower surface heat flow leads to a comparatively thick continental crust (35 km), and correspondingly increased thickness in the thrust section, but the general patterns of fluid flow are similar to those illustrated. Some results for this model will be presented in a separate paper dealing with heat budgets and *PTt*-paths during regional metamorphism.

Table 1: Notation and typical values used in the models

Variable		Value	Unit
A	radiogenic heat production: surface value	2×10^{-6}	W/m^3
C_p^f	specific heat of fluid	1046	J/kg/K
C_p^m	specific heat of the medium (fluid + solid)	880	J/kg/K
g	acceleration of gravity	9·8	m/s^2
k_c	thermal conductivity of the medium	2·25	W/m/K
$\bar{k}_\phi$	tensor of rock permeability		m^2
$k_{\phi 0}$	reference permeability value	10^{-19}	m^2
M_{H_2O}	molar mass of water	18×10^{-3}	kg/mol
n	exponent in permeability–porosity relationship		2
P	fluid pressure		Pa
Q_r	rate of metamorphic reaction		$kg/m^3/s$
q_m	mantle heat flow	45×10^{-3}	W/m^2
T	temperature		°C
T_s	surface temperature	0	°C
u	fluid flux vector		kg m^2/s
U	rate of erosion	0·5, 1, 2	mm/yr
X_f	fluid release or consumption during metamorphism	0·05	kg/kg
z	vertical axis, positive downwards		
z_A	length scale for the decay of A with depth	10^4	m
ΔH_r	enthalpy change for metamorphic reaction	5×10^4	J/mol
α	thermal expansion of fluid	10^{-5}	K^{-1}
μ	fluid viscosity	$1{\cdot}15 \times 10^{-4}$	Pa s
ϕ	rock porosity		m^3/m^3
ϕ_0	reference porosity	5×10^{-4}	m^3/m^3
ϕ_{min}	minimal porosity	10^{-6}	m^3/m^3
ρ	fluid density		kg/m^3
ρ_0	density of fluid at 1 bar, 0°C	1000	kg/m^3
ρ_m	density of the medium	2800	kg/m^3

Metamorphic reactions

The contribution of the latent heat of reaction to the total crustal heat budget is included directly through a corresponding term in the energy conservation, unlike some earlier models that incorporated the heat of reaction using an effective thermal diffusivity and an effective heat capacity for rocks undergoing reaction (e.g. Hanson & Barton, 1989; Peacock, 1989). The amount of heat consumed or liberated in chemical work is proportional to the rates of metamorphic reactions, Q_r. Generally speaking, metamorphic reaction rates are dependent on a large number of factors, including surface reaction mechanisms, the process of product nucleation, and mass transport (e.g. Ague, 2003). The rate at which the heat is added or withdrawn from the rock, however, is thought to be a major control on the overall reaction rates, as suggested by theoretical analysis (e.g. Ridley, 1986; Luttge *et al.*, 2004) and field observations (e.g. Ferry, 1983).

The overall rate of fluid production and consumption, therefore, is modeled as a function of the rate of temperature change within a rock parcel (e.g. Hanson, 1992):

$$Q_r = \frac{X_f \rho_m}{\Delta T} \frac{\partial T}{\partial t} \tag{3}$$

where X_f is the total amount of fluid released or absorbed by the rock over the characteristic temperature interval for reactions, ΔT. Hanson (1997) used an identical expression, but considered only fluid production (positive values of Q_r). In our model, the sign of the temperature change determines the direction in which hydration or dehydration reactions proceed in a particular rock parcel: endothermic dehydration reactions require the addition of heat, i.e., $\partial T/\partial t > 0$, whereas exothermic hydration reactions occur when $\partial T/\partial t < 0$.

The compositional variation of crustal rocks and individual minerals will lead to dehydration (or hydration)

Table 2: List of model runs

Model description	Erosion rate (mm/yr)	Figure
1. No fluid production		
Reference permeability $k_{\phi 0} = 10^{-19}\,m^2$	0	Fig. 2a–c
Background permeability $k_{\phi} = 10^{-20}\,m^2$	0	—
2. Fluid production at reference permeability $k_{\phi 0}$		
Retrograde and prograde reactions	0	Fig. 3a–c
	1	Fig. 4a–d
	0·5, 2	—
No retrograde reaction	1	—
Initial thermal relaxation 0·15 Myr	0	Fig. 3d
3. Fluid production at variable background k_{ϕ}		
$k_{\phi} = 10^{-17}\,m^2$	1	Fig. 5a
$k_{\phi} = 10^{-18}\,m^2$	1	Fig. 5b
$k_{\phi} = 10^{-20}\,m^2$	1	Fig. 5c–d
4. Large-scale anisotropy		
$k_{\phi x} = 10^{-19}\,m^2$; $k_{\phi z} = 10^{-20}\,m^2$	0	Fig. 6a–b
$k_{\phi x} = 10^{-18}\,m^2$; $k_{\phi z} = 10^{-20}\,m^2$	0	—
5. Horizontal barriers		
$x = 0$–60 km, $z = 40$ km; background $k_{\phi} = 10^{-19}\,m^2$	0	Fig. 7a–b
$x = 40$–120 km, $z = 40$ km; background $k_{\phi} = 10^{-19}\,m^2$	0	Fig. 7c–d
$x = 40$–120 km, $z = 40$ km; background $k_{\phi} = 10^{-18}\,m^2$	0	—
6. Vertical permeable zones		
$x = 17$–$18{\cdot}5$ and 33–$34{\cdot}5$ km, $z = 0$–40 km	0	Fig. 8a–b
	1	Fig. 8c–d
7. Permeability contrasts produced by metamorphism		
	0	Fig. 9a–d
	1	Fig. 9c
8. Temperature-dependent k_c	0, 1	—
9. Alternative thermal structure		
$q_m = 35 \times 10^{-3}\,W/m^2$; $A = 3 \times 10^{-6}\,W/m^3$	0, 1	—
10. Porosity exponent $n = 3$	0	—

over large temperature intervals. The lower and upper limits of the interval used here, 200 and 700°C, correspond to the temperature range of low-grade metamorphism to upper amphibolite facies. The maximum amount of water that may be released or consumed during metamorphism is 5 wt % over the entire temperature interval $\Delta T = 500$°C. The source of the fluid produced in dehydration reactions is the chemically bound water stored in the hydrous minerals. We model the initial content of bound water in crustal rocks as a function of the initial temperature distribution. The assumed maximum bound water content is 5 wt %. Rocks with initial temperatures below 400°C are fully hydrated; the water content of rocks at $T > 400$°C drops linearly from 5 wt % to zero over a temperature interval of 400–700°C. Dehydration reactions are permitted only in rocks with non-zero water contents. Hydration reactions are allowed to proceed until the maximum water content, 5 wt %, is reached.

The contribution of metamorphic reactions to the total heat budget of the model is determined by the last term of equation (1) involving the latent heat of reaction, ΔH_r. Reported estimates for the latent heat of metamorphic reactions vary mostly in the range of 30–75 kJ/mol H_2O (Peacock, 1987; Connolly & Thompson, 1989; Connolly, 1997). The latent heat of reactions that involve CO_2 may be even higher, as suggested by the study of metamorphic rock samples by Ferry (1983). For simplicity, we assume that the fluid released or consumed is pure water, and use a representative value for the latent heat of reaction, 50 kJ/mol H_2O. Our results, therefore, represent a conservative estimate for the effect of reactions on the thermal evolution of a metamorphic terrane.

Conservation of mass and momentum

The mass conservation law for a compressible fluid contained in the pore space of a solid matrix relates the changes in fluid mass to the rate of fluid production or consumption in metamorphic reactions, as well as the variations in fluid density and matrix porosity. The rate of fluid production or consumption is determined by metamorphic reaction rates, Q_r:

$$\nabla \cdot \mathbf{u} = Q_r - \frac{\partial(\phi\rho)}{\partial t}. \quad (4)$$

The fluid mass flux $\mathbf{u}$ is defined as the product of fluid (porous) velocity and density:

$$u = \rho\phi v.$$

The momentum conservation equation for fluid is Darcy's law:

$$\mathbf{u} = -\frac{\rho\bar{k}_\phi}{\mu}(\nabla P - \rho\mathbf{g}) \quad (5)$$

where $\bar{k}_\phi$ is a tensor of rock permeability, μ_f is the dynamic viscosity of fluid, P is the fluid pressure, and $\mathbf{g}$ is the vector of gravitational acceleration.

Permeability

Rock permeability is one of the major factors that control the character of fluid flow in the crust, and one that is most poorly known. The permeability values of upper crustal rocks derived from laboratory and *in situ* measurements range over at least six orders of magnitude (Brace, 1980). The middle and lower crust permeability may only be inferred indirectly from fluid fluxes recorded by rock chemistry, studies of the pore network preserved in exhumed deep crustal rocks, or from numerical simulations [see Manning & Ingebritsen (1999) for further details and references]. The suggested values for middle and deep crustal permeability vary from $10^{-17}\,m^2$ to $10^{-21}\,m^2$, and result in contradictory conclusions about fluid pressures and the regime of fluid flow at depth (e.g. Walther & Orville, 1982; Etheridge *et al.*, 1983). In an attempt to resolve these contradictions, Walder & Nur (1984) suggested that permeability and porosity in the deep crust should be regarded as dynamic parameters, constantly evolving in response to hydrofracturing, subsequent crack closing and healing, and mineral precipitation. Metamorphic permeability should then be viewed as an integrated value, with many transient variations averaged over space and time. Manning & Ingebritsen (1999) proposed $\sim 10^{-18{\cdot}5\pm1}\,m^2$ as such an integrated estimate for the middle and deep crust permeability based on metamorphic fluid flux data and geothermal data. We assume their model for this study and use $10^{-19}\,m^2$ as the reference crustal permeability $k_{\phi 0}$. In addition, we construct models with $k_{\phi 0}$ equal 10^{-17}, 10^{-18} and $10^{-20}\,m^2$ to test the effect of the background permeability on fluid flow.

The surface permeability in all of our models is kept at $10^{-16}\,m^2$; the upper crustal k_ϕ drops exponentially with depth with the characteristic length scale of 2·5 km until the background value for the particular model is reached. For our reference model, the background value of $10^{-19}\,m^2$ is reached at about 20 km depth (Fig. 1d); we will generally refer to crustal rocks below this depth as 'deep crust' or 'deep crustal rocks' and to shallower depths as 'upper crustal rocks'. The permeability below the base of the crust is reduced by two orders of magnitude from the background value between the 700°C and 800°C isotherms; rocks with temperature exceeding 800°C are assumed impermeable.

Evolution of permeability

The temporal evolution of permeability, and functionally related porosity, is included via two mechanisms: (1) hydrofracturing of crustal rocks at fluid pressures elevated above the rock strength threshold; (2) production and consumption of porosity in metamorphic hydration and dehydration reactions.

Hydrofracturing and subsequent fracture sealing in crustal rocks is well documented from field observations as well as laboratory measurements (e.g. Ramsay, 1980; Ague 1994; Wong & Zhu, 1999; Miller *et al.*, 2003). The fluid pressure in excess of the sum of the least principal stress (i.e. the lithostatic burden of the rock column) and the tensile strength of the rocks (0·01–0·03 GPa) results in brittle fracturing, release of fluid and the associated decrease in fluid pressure. Our numerical models simulate hydrofracturing by transient porosity–permeability increase in response to fluid pressure elevated above the critical value. A conservative estimate of the amount of permeability production by fracturing is determined by iterative adjustment of permeability, porosity, and corresponding fluid flux values, until fluid pressure is brought just below the critical value. This procedure is slightly different from that employed by Hanson (1997), who derived the value of post-fracturing permeability corresponding to lithostatic fluid pressure from Darcy's Law.

Metamorphic dehydration and decarbonation reactions typically result in mineral volume reduction and corresponding increase of porosity, whereas hydration and carbonation reactions lead to an increase of solid volume and clogging of pore space (e.g. Rumble & Spear, 1983; Connolly, 1997; Zhang *et al.*, 2000; Tenthorey & Cox, 2003). The analysis by Balashov & Yardley (1998) suggests that the rates of porosity creation by metamorphic reactions are likely to overcome the collapse of porosity by deformation. The prograde metamorphic reactions will thus be accompanied by permeability enhancement, whereas retrograde reactions will tend to decrease permeability. We model the porosity–permeability evolution after the muscovite dehydration reaction, with a solid

volume change of −5 cm^3/mol H_2O. This value is a conservative estimate, and is 2–5 times lower than the solid volume change for chlorite model reactions used by Connolly (1997). We limit the increase in permeability in the deep crust to $10^{-18}\,m^2$, based on the data compilation by Ingebritsen & Manning (1999); the permeability reduction is terminated at $10^{-21}\,m^2$, which corresponds to the lowest measured permeability of crystalline rocks (Brace, 1980).

The collapse of porosity as a result of compaction and the corresponding permeability evolution are not included in this modeling, or in most of the previous 2-D models of crustal-scale fluid flow (e.g. Garven & Freeze, 1984*a*; Hanson, 1995, 1997). Two-phase models of fluid flow with permeability–porosity evolution commonly deal with compaction-driven flow in sedimentary basins (e.g. Connolly & Podladchikov, 2000; Morency *et al.*, 2007), although 1-D metamorphic models also exist (e.g. Connolly, 1997). The porosity–permeability evolution is likely to be most important in the earliest stages of the orogen history during the emplacement of the thrust sheets; it will lead to the gravitational collapse of porosity and the expulsion of fluid from buried sediments and low-grade metamorphic rocks in the underlying plate (e.g. Koons & Craw, 1991). In our modeling, the 0·5 Myr delay between thrust emplacement and the start of the simulations is likely to encompass the most intensive period of compaction. By this time, the porosity–permeability structure within the thrust section is assumed to equilibrate, and conform to the reference depth-dependence curve used in our modeling (Fig. 1d). This depth-dependent profile based on the model by Manning & Ingebritsen (1999) is likely to represent the temporally and spatially integrated response of dynamic permeability and porosity to the various divergent processes occurring in the deep crust: crack opening and healing, porosity change as a result of deformation and mineral precipitation, etc. Even in our relatively simple model without the explicit consideration of rock deformation processes, the use of this generalized permeability structure should make it possible to reproduce the first-order behavior of crustal-scale fluid flow.

Porosity–permeability relationship

The functional relationship between porosity and permeability that is required to complement equations (4) and (5) is not well known. A number of proposed functions commonly include a power-law dependence of permeability on porosity (e.g. Connolly, 1997; Wong & Zhu, 1999). In this study, we use the relationship suggested by Walder & Nur (1984):

$$k_\phi = k_{\phi 0}\left(\frac{\phi^n - \phi_{\min}^n}{\phi_0^n - \phi_{\min}^n}\right) \qquad (6)$$

where $k_{\phi 0}$ and ϕ_0 are the reference permeability and porosity, $\phi_{\min}$ is the minimal value of porosity, and the exponent n is on average between 2 and 3 (see Table 1 for the specific parameters used in this work). A higher value of n should lead to more rapid changes in permeability in response to small porosity variations; this is sometimes associated with fracturing, or chemical compaction (e.g. David *et al.*, 1994). Our use of $n = 2$ results in a more conservative estimate of the porosity–permeability feedback; in particular, in the case of porosity growth and reduction during metamorphic reactions. The crustal-scale patterns of fluid flow, however, are independent of the choice of n.

Exhumation

Exhumation, when present, is at a constant rate within the flat section of the topography and is slope-dependent in the tapering section; no exhumation occurs away from the topographic elevation ($x > 120$ km). The maximum exhumation rates of 0·5 mm/yr, 1 mm/yr and 2 mm/yr are within the range suggested by England & Thompson (1984), although faster and slower rates are certainly possible. Erosion is stopped when the entire thickness of the emplaced crustal sheet (30 km) is removed.

Equation of state

To form a closed system, equations (1) and (3)–(6) must be supplemented with an equation of state for the fluid. For simplicity, we assume that metamorphic fluids are composed solely of water. This simplification is justified by the fact that the dynamic viscosities of water and carbon dioxide, which is the second most important component in most metamorphic fluids, are not very different under crustal conditions (e.g. Walther & Orville, 1982). In any case, the variations in viscosity and density of H_2O, CO_2 and their mixtures are trivial compared with the possible range of other parameters, such as permeability and porosity. We calculate the densities of water using the Compensated-Redlich–Kwong (CORK) equation of state of Holland & Powell (1991, 1998).

Solution procedure

The model is solved with Matlab using the finite difference method; the grid size is 2·0 km in the horizontal dimension and 0·5 km in the vertical dimension. The time step is 0·01 Myr for temperature, and 0·02 for pressure and fluid flow solvers. The greater time step for pressure is used to expedite the numerical calculations; it is justified by the slow pressure evolution in the system. The typical simulation time for models with erosion is determined by the time required for exhuming a crustal thickness (30 km) in the thrust segment of the model. The simulation time is therefore 30 Myr for an erosion rate of 1 mm/yr, 60 Myr for an erosion rate of 0·5 mm/yr and 15 Myr for an erosion rate of 2 mm/yr. At each time step, the energy conservation equation is solved with the Crank–Nickolson scheme and

the resultant temperature distribution is used in an iterative solution search for a system composed of mass conservation, momentum conservation and the CORK equation, until mutually consistent distributions of fluid pressure, density, and fluid fluxes are obtained. If fluid pressure is found to exceed the fracturing threshold, the permeability and porosity are iteratively increased within the domain of elevated pressure, and new solutions for the fluid pressure, density and fluid fluxes corresponding to the enhanced permeability–porosity structure are obtained. The permeability–porosity–pressure adjustment is conducted over a single time-step, as the time scale of hydrofracturing is thought to be very small (~10–100 yr) in comparison with the heat conduction and fluid flow time scales (e.g. Sleep & Blanpied, 1992). The solution procedure was tested with mass-balance calculations: the cumulative mass-balance error (i.e. the unaccounted for variation in fluid mass in each cell divided by the total fluid mass in a cell) within the model area was of the order of 10^{-8} kg/kg. The results were found to be invariant for changes in the time step or grid spacing.

RESULTS

Thermal buoyancy, metamorphic reactions and exhumation

Fluid convection in the absence of reaction

In the simplest case when metamorphic reactions and exhumation are absent, the model topography along with the thermal and fluid density gradients within the thrust section drive the counterclockwise circulation of fluid, in agreement with many previous models (e.g. Garven & Freeze, 1984*b*) and the results reported by Hanson (1997; Fig. 2a and b). At early times (Fig. 2a), the slope of the isotherms is from left to right as a result of thrusting. The temperature in the lower plate in the left part of the model increases with time as a result of thermal conduction and the doubled radiogenic heat production within the thickened crust, such that the slope of the isotherms gradually decreases with time. After 10 Myr (Fig. 2b), the inverse section of the geotherm in the thrust area is equilibrated; the isotherms are roughly parallel to the surface in the entire model section after 30 Myr.

The fluid pressures are near the hydrostat in the entire crustal section because of the interconnected porosity structure and the absence of any mechanisms for porosity or permeability evolution in this simulation. Maximum fluid flux below 20 km depth is about 0·06 kg/m^2/yr at 1 Ma and 0·02 kg/m^2/yr at 10 Ma [the latter value is almost identical to that in a similar model by Hanson (1997), 0·018 kg/m^2/yr]. The time-integrated fluid fluxes below 20 km depth are of the order of 10^2 m^3/m^2 for the crustal permeability of 10^{-19} m^2 (Fig. 2c). Higher fluxes of 10^3–10^4 m^3/m^2 are attained in the shallower crust underneath the topographic slope. The highest fluxes of 10^5 m^3/m^2 are limited to the uppermost crust within 5 km, where permeability is of the order of 10^{-16}–10^{-17} m^2. Different values for the background permeability will scale the fluid fluxes and the time-integrated fluxes, as predicted by Darcy's Law, but will not change the fluid flow pattern, even at $k_\phi = 10^{-20}$ m^2.

Upward flow as a result of metamorphic dehydration

The introduction of metamorphic hydration and dehydration reactions has a significant effect on the fluid flow. The results of modeling for a background permeability of 10^{-19} m^2 are shown in Figure 3a–c. The flow is upward in most of the crustal section and is driven by fluid influx from metamorphic reactions occurring in the deep crust.

The metamorphic reaction rates are highest early in the thrust history, when thermal contrasts are strong and temperature changes are rapid (Fig. 3a). At this stage, the colder sections of the buried lower plate beneath the fault zone are heating rapidly (0·07°C/10^3 yr at 0·5 Ma); they are a major source of fluid released in metamorphic dehydration reactions. This fluid is expelled upwards, and is partially drawn into the hanging wall of the thrust, which is a major zone of retrograde hydration; the rate of cooling in this area is about −0·06°C/10^3 yr at 0·5 Ma. The other zone of hydration that develops at this early stage of the orogenic history is located at the side of the model away from the thrust ($x = 100$–240 km, $z = 20$–35 km). The cooling in this area is due to 2-D heat equilibration between the relatively cool, but rapidly heating thrust region, and the near steady-state temperature field in the right flank of the model. The cooling rate in this area is very slow in comparison with that within the thrust core; the highest value is attained in the zone of maximum isotherm inflection and is only −0·01 °C/10^3 yr at 0·5 Ma.

With time, the rates of temperature change and corresponding reaction rates decrease as a result of thermal relaxation (Fig. 3b). By about 5 Ma, despite continuing cooling within the hanging wall of the thrust, the rocks there become fully hydrated and retrograde reactions stop (see Fig. 2c for the map of initial bound water content). The zone of prograde reaction gradually widens; the rate of fluid production, however, continually decreases, and is about 3–4 times lower at 10 Ma than at 1 Ma. Retrograde reaction in the right part of the model, although extremely slow, will persist as long as there are thermal contrasts between the thickened crust region and the unperturbed crustal section.

The influx of fluid released by metamorphic dehydration reactions in the deep crust elevates fluid pressures above the hydrostatic level (Fig. 3a and b). The fluid pressure at 50 km depth in the thrust region is above 0·6 GPa at 1 Ma, which is almost 50% higher than the hydrostatic pressure (Fig. 2a). As metamorphic reaction slows down with time, the fluid pressure gradually decreases; it drops to 0·5 GPa

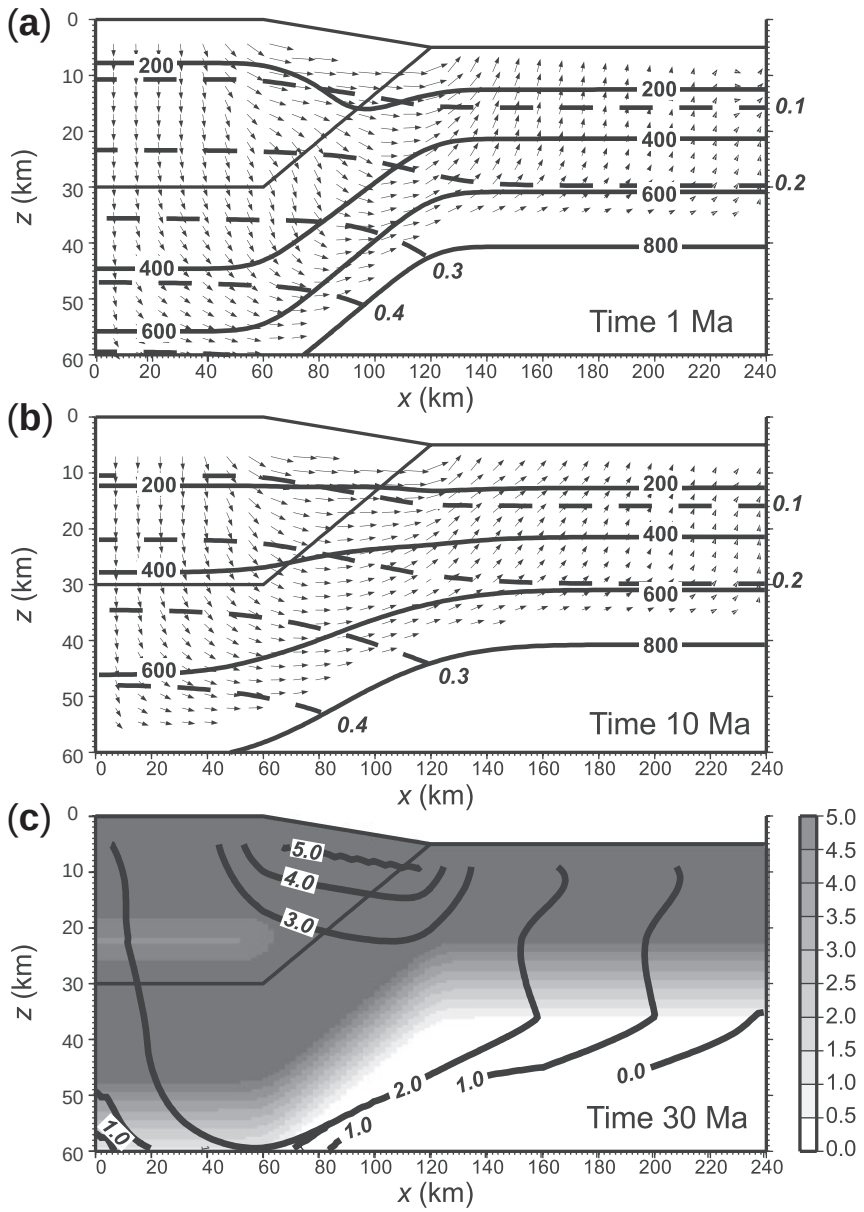

Fig. 2. Results for a model with no fluid production. (a) Arrows depict fluid mass flux after 1 Myr; length of arrows is scaled for visibility with logarithmic scale; for clarity, mass flux in the upper 5 km is not shown. Continuous lines are isotherms in °C. Dashed lines are fluid pressure in GPa (values in italics). Maximum fluid flux below 20 km depth is ~0·06 kg/m^2/yr. (b) Same as in (a), after 10 Myr. Maximum fluid flux below 20 km depth is ~0·02 kg/m^2/yr. (c) After 30 Myr. Shading depicts bound water content in the constituent minerals (wt %). Continuous lines are integrated volume fluid fluxes ($\log_{10}$ m^3/m^2). As no fluid is produced or consumed in this model, the bound water content at 30 Myr is identical to the initial water content.

at 50 km depth in 10 Myr, and is only slightly above hydrostatic pressure after 30 Myr.

The time-integrated fluid fluxes attained with this model are considerably higher than the fluxes in the model with no metamorphic reactions. In most of the deep crust (below 20 km depth) the integrated fluxes are of the order of 10^3 m^3/m^2 (Fig. 3c). They become 10–100 times higher in the upper crust, where permeability increases from 10^{-19} to 10^{-16} m^2. The very high flux in the uppermost crust below the topographic slope is mainly due to the sub-surface flow driven by topographic elevation. Figure 3c shows the distribution of bound water content in crustal rocks after 30 Myr of thrust evolution. Most of the lower plate rocks that initially were fully hydrated (Fig. 2c), have lost up to 3–4 wt % of their water content. The rocks within the core of the thrust that had slightly reduced water content before the beginning of the simulation became fully hydrated over the first 5 Myr, and then

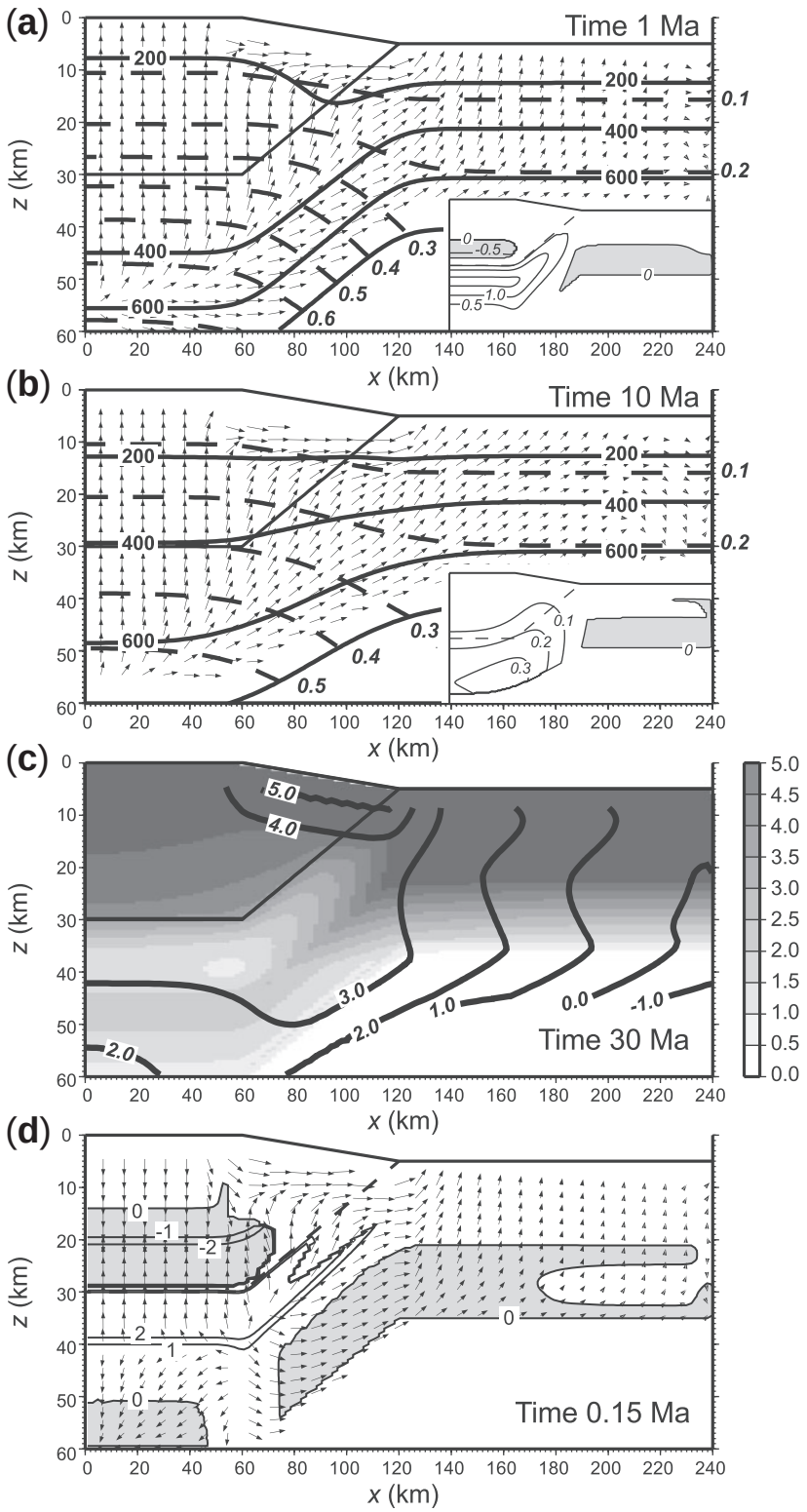

Fig. 3. Model results for the case with fluid production, no exhumation. (a) Fluid mass flux after 1 Myr. Inset shows fluid consumption (shaded areas) and production, in kg/m^3/10^5 yr. Maximum fluid flux below 20 km is ~0·22 kg/m^2/yr. (b) Same as (a), after 10 Myr. Maximum fluid flux below 20 km is ~0·07 kg/m^2/yr. (c) Bound water content in the constituent minerals of the rocks (wt %, shading) and integrated volume fluid fluxes, in $\log_{10}$ m^3/m^2 (lines) after 30 Myr. (d) Fluid production (in kg/m^3/10^5 yr) after 0·15 Myr for a model preceded by short period (0·15 Myr) of conductive relaxation of the initial sawtooth geotherm. Intensive hydration leads to transient downward flow of fluid in the thrust core and in the lower plate.

started to lose water again as retrograde reaction in this area was replaced by prograde metamorphism.

Metamorphic reactions were found to exert controls on temperature evolution. The exothermic hydration reactions produce substantial amounts of heat, thus retarding the temperature decrease in the regions where the reactions take place. Endothermic dehydration reactions, on the other hand, consume heat and slow down the rate of heating of the rocks. As seen from a comparison of Figs 3b and 2b at 10 Myr the 400°C and 600°C isotherms in the model with reaction are at least 2 km deeper than in the model with no reaction. We will address the effect of reaction on the temperature regime of a model orogenic setting in more detail in a separate paper.

Metamorphic flux vs buoyancy flux

The mostly upward fluid flow in the model with metamorphic reactions, as well as elevated pressures, demonstrates that in the parameter space of the model, the flux of fluid driven by pressure gradients resulting from metamorphic reactions (metamorphic flux) predominates over the flux produced solely by temperature-induced density gradients (buoyancy flux). Metamorphic dehydration leads to the expulsion of fluid from areas undergoing prograde reaction and the predominantly upward flow of fluid towards the crustal surface. The effects of hydration reactions on fluid flow, on the other hand, are opposite to those produced by metamorphic dehydration: retrograde reaction areas may act as fluid sinks, and under certain conditions lead to downward and up-temperature flow.

The conditions for which fluid expulsion consequent to metamorphic dehydration reactions may overcome the buoyancy flux have been discussed by Hanson (1992). A similar analysis can be made for the case of the metamorphic flux resulting from hydration.

Darcy's Law (or momentum conservation equation) predicts that the flux of fluid will occur in response to gradients in fluid pressure in excess of the hydrostat. If fluid pressure gradients are caused by temperature contrasts, the resulting buoyancy flux may be approximated as

$$u_{\mathrm{B}} = \frac{\rho k_\phi}{\mu}\rho_0 \alpha \Delta T g \tag{7}$$

where ρ is the fluid density, k_ϕ is permeability, μ is fluid viscosity, ρ_0 is fluid density at 1 bar and 0°C, α is the coefficient of thermal expansion, ΔT is the temperature difference responsible for the flow, and g is the acceleration due to gravity (Hanson, 1992).

The fluid flux resulting from metamorphic reaction occurring in a depth interval Δz may be roughly estimated from the mass conservation equation

$$u_{\mathrm{MR}} = Q_r \Delta z = \frac{X_{\mathrm{f}}\rho_{\mathrm{m}}}{\Delta T}\frac{\partial T}{\partial t}\Delta z. \tag{8}$$

When metamorphic flux exceeds buoyancy flux, $u_{\mathrm{MR}} > u_{\mathrm{B}}$, the fluid flow is dominated by reaction. Combining the two expressions, we obtain the following condition:

$$\beta \frac{\partial T}{\partial t} > k_\phi \Delta T \frac{\Delta T}{\Delta z} \tag{9}$$

where the coefficient $\beta = \mu X_{\mathrm{f}}\rho_{\mathrm{m}}/(\rho\rho_0\alpha g)$. Therefore, the metamorphic flux is likely to control the fluid flow pattern when the temperature changes $\partial T/\partial t$ driving the reaction are rapid ($\partial T/\partial t > 0$ in case of hydration, and $\partial T/\partial t < 0$ in case of dehydration). The other conditions for the dominance of metamorphic flux include low permeability of the rock (k_ϕ), small temperature contrasts producing the buoyancy flux (ΔT), and relatively high thermal gradients within the region undergoing metamorphic reaction ($\Delta T/\Delta z$). When these conditions are met and metamorphic reaction leads to rock dehydration, the fluid will be expelled towards the surface in the direction of decreasing temperature for the case of a normal geotherm, or in the direction of locally increasing temperature, if the geotherm is inverted in the crustal region above the dehydrating area (e.g. Fig. 1c). If metamorphic reaction leads to fluid consumption during hydration of minerals, the fluid flow will be in the direction of elevated, but gradually decreasing, temperature.

The rates of temperature change in our model vary from 10^{-2} to less than 10^{-4}°C/10^3 yr, or 10^{-12}–10^{-14} °C/s, consistent with the range of temperature change during regional metamorphism discussed by Hanson (1992). The coefficient β is of the order of 10^{-4} m s °C for water densities characteristic for crustal conditions (500–1000 kg/m^3; see Table 1 for other parameter values). The left side of equation (9) is therefore in the range 10^{-15}–10^{-18} °C °C m. On the other hand, the temperature contrasts during regional metamorphism may reach hundreds of °C, with thermal gradients of the order of 0·02–0·03°C/m. From this it follows that at the reference permeability of 10^{-19} m^2, the metamorphic flux will almost always exceed the buoyancy flux. Because in the orogenic collisional setting temperature tends to increase in most of the crust as a result of the relaxation of the perturbed geotherm and elevated radiogenic heating, the metamorphism is dominated by dehydration. The typical fluid flow pattern in most of the orogen is likely to be sub-vertical, towards the surface. In the isolated areas where temperature is decreasing (e.g. in the thrust core and in the flanks of the thickened crust section), the up-temperature flux into hydrating areas will compete with the dehydration flux.

In Figure 3b, the hydration-dominated, up-temperature flow can be seen at the bottom of the crust flanking the orogen, in the vicinity of the right boundary of the model. The extremely slow cooling in this area leads to a downward flow, as the flux of metamorphic fluid produced

within the thrust area does not reach this most distant region. With time, as the fluid flux from dehydration diminishes as a result of decreasing heating rates, the zone of the downward flow in the right part of the model will expand.

Highly exotic, if transient, flow patterns may develop under conditions of extremely high heating and cooling rates that may occur in the early stages of collision with fast convergence rates. We examine a special case of such rapid convergence with a model in which the conductive relaxation of the initial sawtooth geotherm within the thrust area occurs over 0·15 Myr instead of 0·5 Myr, as in other models. The fluid flow pattern for this model after 0·15 Myr is shown in Fig. 3d. The high rates of crustal cooling in the hanging wall of the thrust and in the bottom of the lower plate result in extensive downward flux owing to hydration. At later times, the thermal gradients smooth out, and regions of hydration reactions contract, whereas the regions of dehydration expand as a result of enhanced radiogenic heat production in the thrust area. By 0·3 Ma, the influx of fluid produced by dehydration overcomes the rate of fluid consumption in retrograde reactions and fluid flow becomes upward in most of the upper plate, similar to what is shown in Fig. 3a.

Exhumation

Rock advection via exhumation does not significantly alter the relative proportions of metamorphic and buoyancy fluxes at the reference permeability value in the first 10 Myr of thrust evolution. The fluid flow pattern up to this time is similar to that in the model without exhumation (Fig. 4a). The major effect of exhumation is to accelerate the thermal evolution of the model orogen. The relatively fast erosion rate of 1 mm/yr acting over 10 Myr transfers the 400°C and 600°C isotherms almost 10 km closer to the surface in comparison with their positions in the model without exhumation (compare Figs 3b and 4a). In fixed reference frame coordinates, the overall rate of temperature change in the model crust section is therefore significantly increased by erosion. This rate, however, is different from the rate of heating or cooling within a moving rock parcel; the latter determines the rate of metamorphic reaction within the exhumed rocks. A rock in the lower plate of the thrust on its exhumation path is first heated as a result of the re-equilibration of the faulted geotherm, and then starts to cool as erosion brings it closer towards the surface. At 10 Ma, a hydration zone starts to develop in the vicinity of the fault zone at 20 km depth (compare insets in Figs 4a and 3b). As more of the deep rock is brought towards shallower parts of the crust, the zone of hydration expands and the zone of dehydration reactions at the base of the crust diminishes. At 17 Myr, the underthrust rocks that were initially 30–40 km below the surface are brought to 13–23 km depth; the rates of cooling and hydration within these rocks become strong enough to produce downward flow of fluid in the shallow crust at the center of the thrust zone (Fig. 4b). In later times, most of the fluid flow in the central part of the model thrust is downward, in the up-temperature direction. In contrast, if no hydration reactions are allowed to proceed in this model with exhumation, the fluid flow is upward over the entire exhumation history (not shown).

The time-integrated fluid fluxes after 30 Myr are of the order of 10^3 m^3/m^2 below 10 km depth and 10^4 m^3/m^2 in the uppermost crust beneath the topographic slope (Fig. 4c). Figure 4d shows the temporal evolution of the total time-integrated fluxes in this model: as deep rocks move upward with advection, the amount of fluid that originated within these rocks or passed through them on its way to the surface gradually increases. At the same time, the rocks in the shallow portions of the crust that underwent large fluxes early in the thrust history are continually removed from the system by erosion. At 30 Ma, the rocks in the upper 10 km of the thrust zone (initially at 30–40 km depth) are fully hydrated, as in the model without erosion (Fig. 3c). In the former case, however, all the water is acquired through intensive retrograde reaction in the last 15–20 Myr of the thrust evolution. In a similar model with exhumation but no retrograde hydration allowed, the rocks in the upper 10 km of the thrust zone will retain on average only 3 wt % of water by the end of the simulation (not shown).

At different exhumation rates ($U = 2$ mm/yr and 0·5 mm/yr, Table 2), the patterns of fluid flow are found to be very similar to those shown in Fig. 3. The temporal evolution of the flow, however, reflects the differences in the lifetime of the model orogen: 15 Myr for $U = 2$ mm/yr and 60 Myr for $U = 0{\cdot}5$ mm/yr. In particular, exhumation-produced downward flow, as in Fig. 3, in a model with $U = 0{\cdot}5$ mm/yr develops at about 26 Ma instead of 17 Ma. The time-integrated fluxes in models with different erosion rates are also similar, albeit accumulated over very different time-scales (e.g. 10^3 m^3/m^2 below 20 km depth over 60 Myr, for $U = 0{\cdot}5$ mm/yr).

The effect of the background permeability

The major control on the interplay between the metamorphic flux and the buoyancy flux is permeability, which may vary over many orders of magnitude in crustal rocks. In Fig. 5a–d we present the results for models with background permeabilities of 10^{-17}, 10^{-18} and 10^{-20} m^2, exhumation rate of 1 mm/yr, and metamorphic reactions that consume or release 5% of water over a temperature interval of 500°C.

At high background permeability, the flow is dominated by buoyancy forces (Fig. 5a). The fluid pressures are near hydrostatic and fluid is circulating in the entire crustal section, much as in the case where metamorphic reactions are absent (Fig. 2b).

At a crustal permeability of 10^{-18} m^2, the metamorphic flux is dominant over the buoyancy forces only in the area of the thickest crust, where temperature changes and rates of metamorphic reactions are highest; the flow in the center of the thrust section is therefore in the upward direction (Fig. 5b). Near the flank of the thrust, metamorphic fluid production slows down, fluid pressure drops to hydrostatic levels, and fluid tends to move laterally. At 10 Ma, the fluid pressures are only slightly above hydrostatic. By 20 Ma, as dehydration metamorphism is replaced by hydration in most of the thickened crust section as a result of the fast cooling of the exhumed rocks, the fluid flow in the center of the thrust is downward (as in Fig. 5a; not shown). The fluid circulation in this case is the combined result of the topography-driven density contrasts and the fluid sink provided by hydration reactions occurring in central part of the thrust zone.

With a further decrease in background permeability to 10^{-19} m^2, the metamorphic flux starts to dominate in most of the model crustal section. The fluid is overpressured in

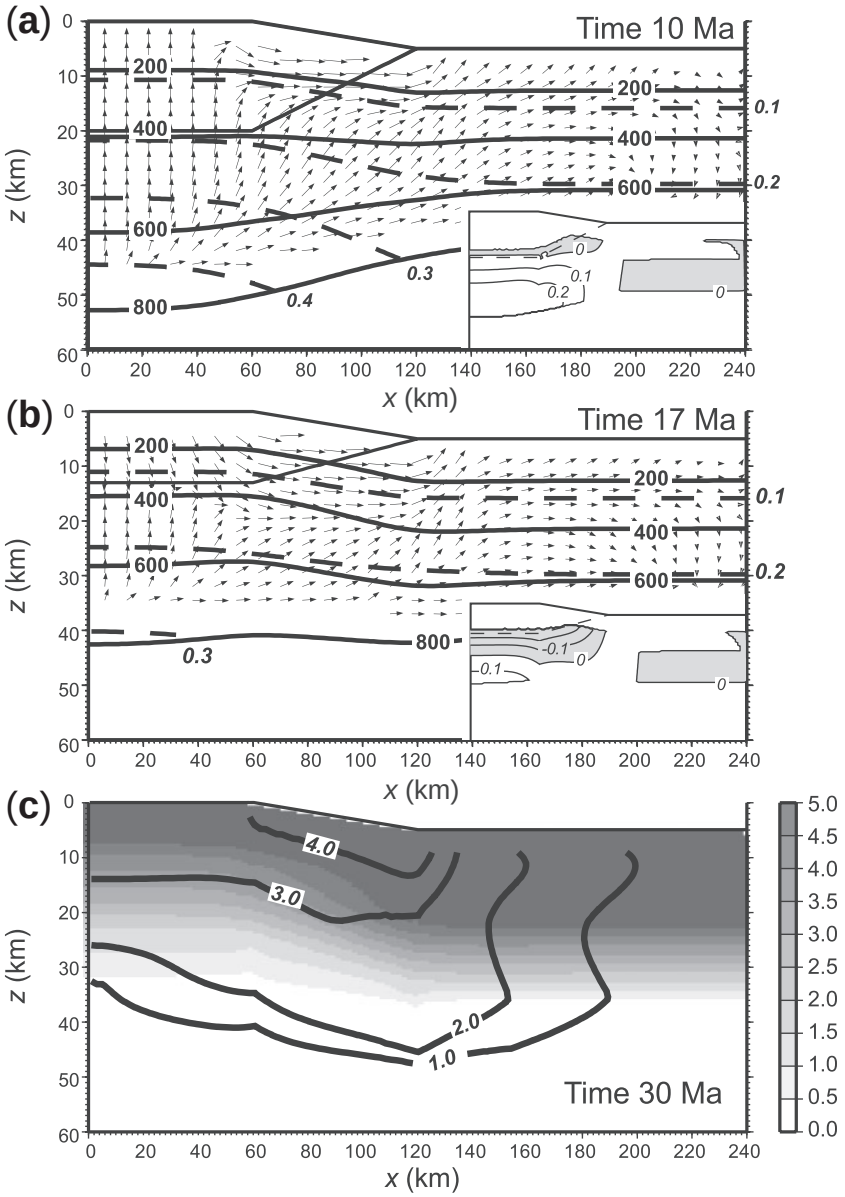

Fig. 4. Model results for the case with fluid production, exhumation rate 1 mm/yr. (a) Fluid mass flux after 10 Myr. Maximum fluid flux below 20 km is ~0·04 kg/m^2/yr. (b) Fluid mass flux after 17 Myr. Maximum fluid flux below 20 km is ~0·02 kg/m^2/yr. (c) Bound water content in constituent minerals of the rocks (wt %, shading) and integrated volume fluid fluxes, in $\log_{10}$ m^3/m^2 (lines) after 30 Myr. (d) Integrated volume fluid fluxes ($\log_{10}$ m^3/m^2) at 5, 7, 10 and 15 Myr.

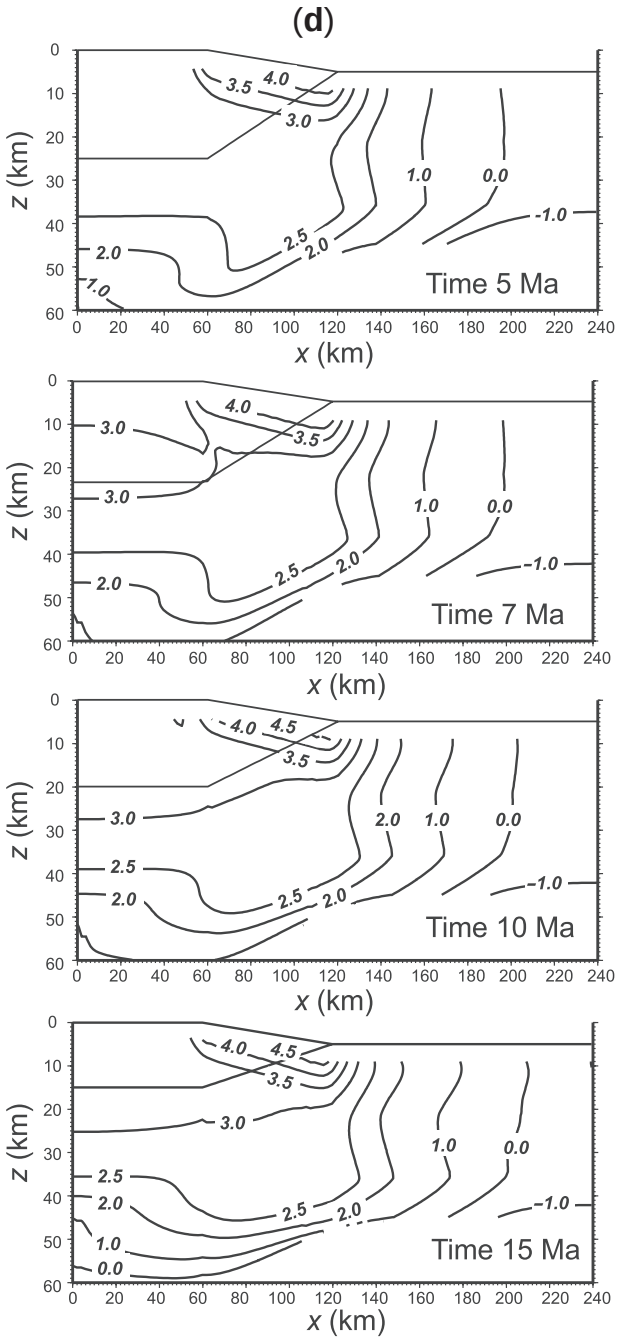

Fig. 4. Continued.

the first 10–15 Myr of the crustal evolution; dehydration metamorphism expels fluid towards the surface. At later times (after 17 Myr), the flow is dominated by hydration reactions, which pull the fluid in the downward, up-temperature direction (Fig. 4a and b).

When the background permeability is at 10^{-20} m^2, the buoyancy flux is negligible in comparison with the metamorphic flux everywhere in the crustal section (Fig. 5c and d). The fluid pressures in the thickest regions of the crust are in excess of lithostatic pressures for over 6 Myr after the start of the simulation. The high pressures lead to hydrofracturing and local permeability–porosity increases in areas of elevated pressure. In the first 1 Myr of the thrust evolution all of the deep crust in the orogenic zone (below 25 km) is hydrofracturing; the minimal permeability that is required to bring fluid pressure below the lithostatic level in the center of the fracturing zone is $\sim 10^{-19.5}$ m^2 (Fig. 5c). As rates of reactions fall with time, the fluid pressure gradually decreases, and the area of hydrofracturing contracts. At 5 Ma, only the crust below 35 km undergoes fracturing, with permeability increasing by $\sim 10^{0.2}$ m^2. Such temporal evolution of hydrofracturing echoes the observed correlations between the abundance of veins in regional metarmophic terranes and the metamorphic grade. Higher grade regions commonly have greater abundance of veins than lower grade regions (e.g. Ague, 1994; Penniston-Dorland & Ferry, 2008); the difference may reflect greater amounts of produced fluid and correspondingly larger orverpressures in higher grade rocks, similar to what happens in our model at early times (Fig. 5a).

At 10 Ma, the fluid pressures are below lithostatic values everywhere in the thrust section; they are, however, significantly higher than in the case with the reference permeability of 10^{-19} m^2 (Fig. 5d). Later in the thrust evolution (after 15–17 Myr), the exhumation-driven retrograde reactions in the central part of the thrust will produce the downward flow of fluid, as in the model with the reference permeability structure (Fig. 4b).

The very low background permeability of 10^{-20} m^2 results in small absolute values of fluid flux in most of the crust, especially away from the hydrofracturing zone. As a result, the flux of fluid expelled from zones of metamorphic dehydration is not large enough to compete successfully with the up-temperature pull exerted on the fluid by the metamorphic hydration zone. The entire right part of the model, therefore, is characterized by downward, up-temperature flow. The magnitude of the flux in this area, however, is very small, of the order of 10^{-3} kg/m^2/yr at 10 Ma. For comparison, the magnitude of the upward flux in most of the thrust section at this time is above 5×10^{-2} kg/m^2/yr.

Anisotropy and spatial heterogeneity in crustal permeability structure

Crustal anisotropy

Anisotropy produced by layering, foliation, lithological contacts, and fracture networks has been suggested to induce horizontal fluid flow as opposed to general upward, or down-temperature flow driven by thermal buoyancy forces (e.g. Skelton, 1996). Large-scale crustal anisotropy has also been proposed by Ingebritsen &

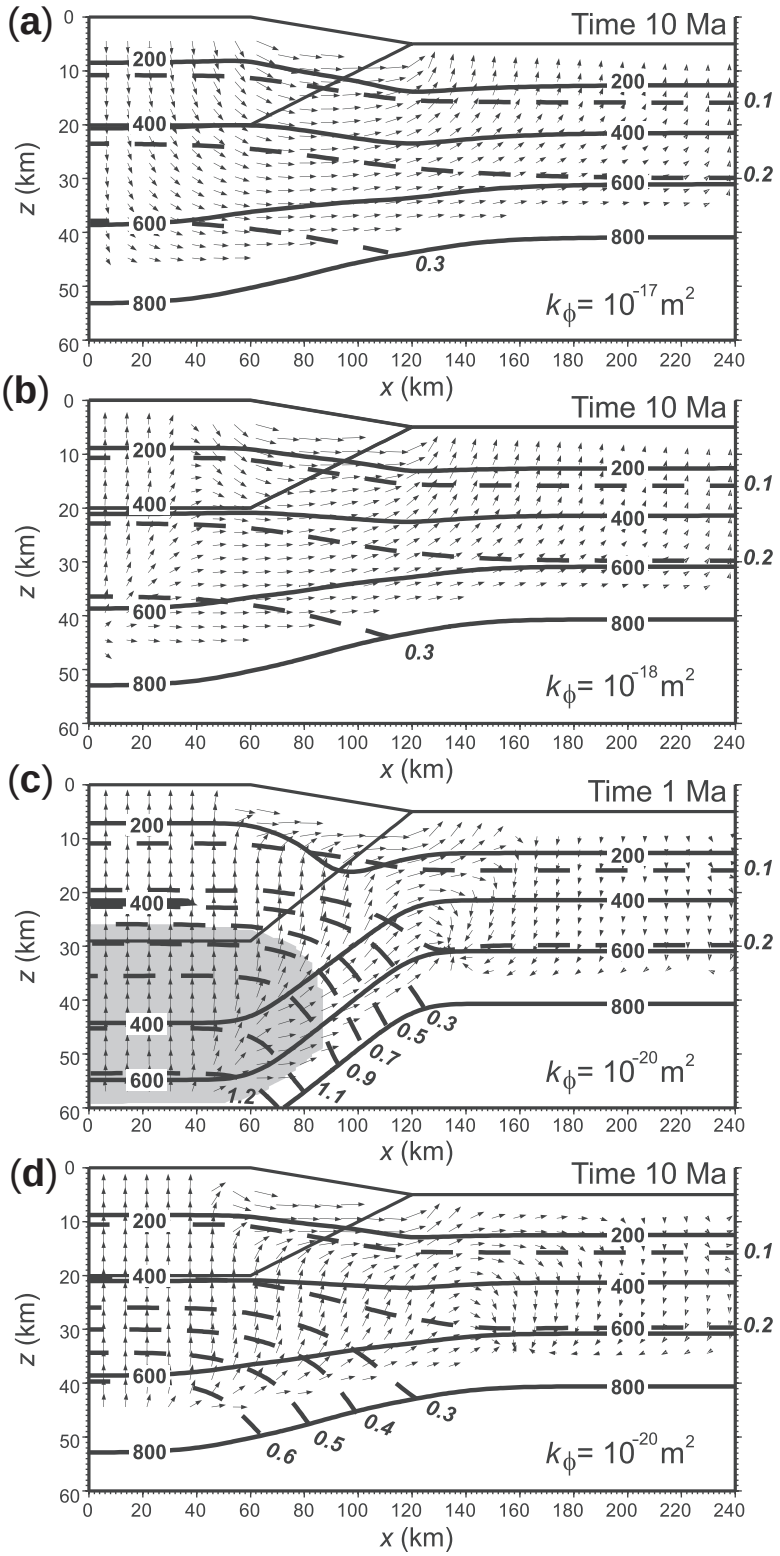

Fig. 5. Model results for variable background permeability, exhumation rate 1 mm/yr. (a) $k_\phi = 10^{-17}$. Fluid mass flux after 10 Myr. Maximum fluid flux below 20 km is ~1·1 kg/m^2/yr. (b) $k_\phi = 10^{-18}$. Fluid mass flux after 10 Myr. Maximum fluid flux below 20 km is ~0·15 kg/m^2/yr. (c) $k_\phi = 10^{-20}$. Fluid mass flux after 1 Myr. Shading denotes the area of hydrofracturing; permeability in the fractured area $k_\phi \sim 10^{-19.5}$. Maximum fluid flux below 20 km is ~0·22 kg/m^2/yr. (d) $k_\phi = 10^{-20}$. Fluid mass flux after 10 Myr. Maximum fluid flux below 20 km is ~0·04 kg/m^2/yr.

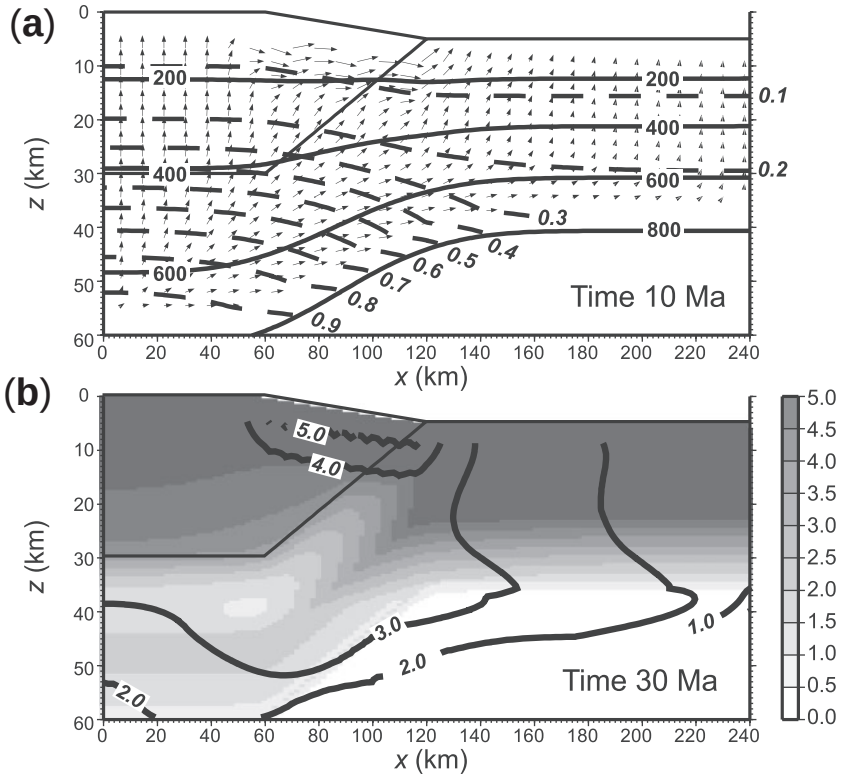

Fig. 6. Model results for anisotropic permeability: $k_{\phi x} = 10^{-19}$ (horizontal component), $k_{\phi z} = 10^{-20}$ (vertical component) in the middle and deep crust, no exhumation. (a) Fluid mass flux after 10 Myr. Maximum fluid flux below 20 km is ~0·1 kg/m^2/yr. (b) Bound water content in constituent minerals of the rocks (wt %, shading) and integrated volume fluid fluxes, in $\log_{10}$ m^3/m^2 (lines) after 30 Myr.

Manning (1999), to explain the apparent paradox between the relatively high deep crustal permeability suggested by metamorphic flow data, and the at least 10 times lower permeability that is required to maintain fluid pressures at near-lithostatic levels in the deep crust. Those workers suggested that the geothermal and metamorphic data are likely to reflect the principal component of the crustal permeability tensor. Layering and foliation in crustal rocks may result in higher permeability in the direction parallel to layering than perpendicular to it. If the layering is sub-horizontal, then the vertical component of the permeability tensor may be significantly smaller than the horizontal component. In this case, the geothermal and metamorphic flow data will reflect the higher permeability component of the tensor, whereas the fluid pressures will be determined by the entire tensor structure. In Fig. 6a and b we present the results obtained with a model that specifically tests this proposition by Ingebritsen & Manning (1999). The background permeability is split into two components: the horizontal component is identical to the reference permeability structure in our default models (i.e. drops exponentially from 10^{-16} m^2 at the surface to 10^{-19} m^2 at 20 km depth as in Fig. 1d); the vertical component decreases at a similar rate from 10^{-16} m^2 at the surface to 10^{-20} m^2 at ~30 km depth. The fluid flow is generally towards the surface, but is slightly enhanced in the horizontal direction (Fig. 6a).

The fluid pressures are considerably elevated compared with a similar model with isotropic permeability (Fig. 3b); they are somewhat above lithostatic values in the first 2 Myr of the thrust evolution (about 10% higher at 1 Ma) and drop to below the lithostat later on as the metamorphic reactions slow down. At 10 Ma, the fluid pressures are about 30–40% lower than lithostatic values (Fig. 6b) and continue to decrease gradually with time. At higher anisotropy ratios, the lateral component of the flow is further enhanced. The amount of pressure elevation is dependent on the values of the horizontal and vertical permeability components, the rate of fluid production and other factors such as thermal gradients resulting from thrusting, radiogenic element content, and exhumation rate.

The time-integrated fluid fluxes at 30 Ma in the model with anisotropy are similar to those in the model with isotropic permeability (Fig. 6b). The area of the highest fluxes in the deep crust, however, has a slightly elongated shape, which is the result of the enhanced sub-horizontal component of the flow.

Barriers to fluid flow

Spatial heterogeneity in the permeability of crustal rocks has long been discussed as another potential mechanism to control and direct fluid flow in the crust (e.g. Oliver, 1996). Low-permeability barriers have been proposed to elevate fluid pressure in crustal segments (e.g. Bredehoeft & Hanshaw, 1968), and to isolate permeable layers, promoting local circulation of fluid (e.g. Etheridge *et al.*, 1984). We test several models with permeability structures that are intended to bar or to divert fluid flow in the deep crust (Fig. 7a–d). The setups are schematic and designed solely for testing the hypotheses of possible downward, up-temperature, or convective flow of fluid resulting from heterogeneous permeability.

In Fig. 7a and b, a barrier layer 1 km thick with permeability 10^{-22} m^2 is placed at the center of the thrust region with a background permeability of 10^{-19} m^2, just above the zone of intensive metamorphic dehydration. The fluid pressure is considerably elevated: at 50 km depth at 1 Ma, it is ~0·1 GPa higher than in a similar model with a homogeneous permeability structure. The pressure elevation is strongest at early times, when the fluid production is greatest. The flow below the low-permeability layer is mainly sideways, parallel to the barrier. At the edge of the layer the flow is upwards, and is strongly focused. The fluid fluxes integrated over 30 Myr are over $3{\cdot}5 \times 10^3$ m^3/m^2 in this area, but the amount of flow through the barrier is very small.

In Fig. 7c and d, a low-permeability layer is placed to the side of the thickened crust region. The pressure elevation is slightly weaker than for the case with the barrier at the center of the thrust as a result of slower fluid production rates at the side of the thrust region. Despite the fact that a partly isolated compartment is created underneath the low-permeable layer, no fluid circulation occurs in this area. Fluid circulation is not observed even when the background permeability in the model with the low-permeability layer is increased to 10^{-18} m^2. Instead, part of the flow moves sub-horizontally to the left edge of the low-permeability layer, and another, smaller component of the flow slowly percolates through the barrier near the point of its contact with the bottom of the crust. In this model, as in the previous one, the major focusing of the flow is at the edge of the low-permeability layer; the integrated fluid flux is greater than $3{\cdot}5 \times 10^3$ m^3/m^2 after 30 Myr.

Flow focusing in fracture zones

Narrow zones of enhanced permeability (i.e. regional fracture zones) are thought to channelize fluid flow and increase time-integrated fluid fluxes to levels that might potentially affect temperature distribution (e.g. Brady, 1988; Chamberlain & Rumble, 1988, 1989; Ague, 1994). In Fig. 8a–d we present the model results for a permeability structure that schematically reproduces such a setting by including two channels 1·5 km wide; the vertical permeability component within the channels is 10^{-17} m^2, the horizontal component is at the background permeability level of 10^{-19} m^2. The resultant flow is strongly focused towards the permeable zones. The time-integrated fluxes after 30 Myr are 10^4 m^3/m^2 within the channels; the maximum values are attained in the depth interval 10–35 km, which corresponds to the top of the dehydration region. The area between the channels is relatively depleted in fluid flow, with time-integrated fluxes below 10^3 m^3/m^2.

In a model with exhumation included, the upper 30 km of the crust is removed over 30 Myr (Fig. 8c and d). As a result, the rocks within the permeable channels that have the highest integrated fluxes in excess of 3×10^3 m^3/m^2 are located at shallow depths (above 20 km) and are exposed on the crustal surface. The upper crustal rocks in the thrust area are fully hydrated as a result of intensive retrograde reaction during the late stages of exhumation. If retrograde reactions are not permitted, the upper crust is considerably dehydrated such that the bound water content is diminished by at least 1·5–2 wt%. The permeable channels in such a model, therefore, cut into mostly dehydrated rock as opposed to the models without retrograde reactions or without erosion.

The integrated flux of 10^4 m^3/m^2 is the maximum flux attained in our models over 30 Myr with a reference permeability of 10^{-19} m^2 and fluid production of 5% over 500°C. In fact, this is the upper limit for the amount of water that can be extracted from a rock column of 60 km height composed of rock with density of 2800 kg/m^3, a mineral-bound water content of 5 wt %, and an average fluid density of 800 kg/m^3. Larger fluxes would require that the fluid be replenished by processes such as subduction (e.g. Breeding & Ague, 2002). We note that the estimated fluxes of ~10^4 m^3/m^2 represent averages over the volume of the conduit regions. If the fluids were further channelized into fractures within these regions, then the fluxes within single fractures could be considerably larger (e.g. Ague, 2003).

Fluid fluxes in excess of 10^4 m^3/m^2 might affect the temperature distribution through advective heat transport over short time-scales (Brady, 1988; Chamberlain & Rumble, 1989). In our models, however, this effect is minor; the temperature change as a result of fluid advection is less than 15°C in the first 5 Myr. Larger fluid fluxes (and correspondingly stronger thermal perturbations) might be attained if the permeability contrasts within the fracture zones are higher, and if larger sources of fluid are available.

Permeability evolution as a result of metamorphic reaction

Finally, we consider the case of heterogeneous permeability developed as a result of metamorphic reactions. Permeability tends to increase in rocks that undergo prograde metamorphism because the volume of the reaction

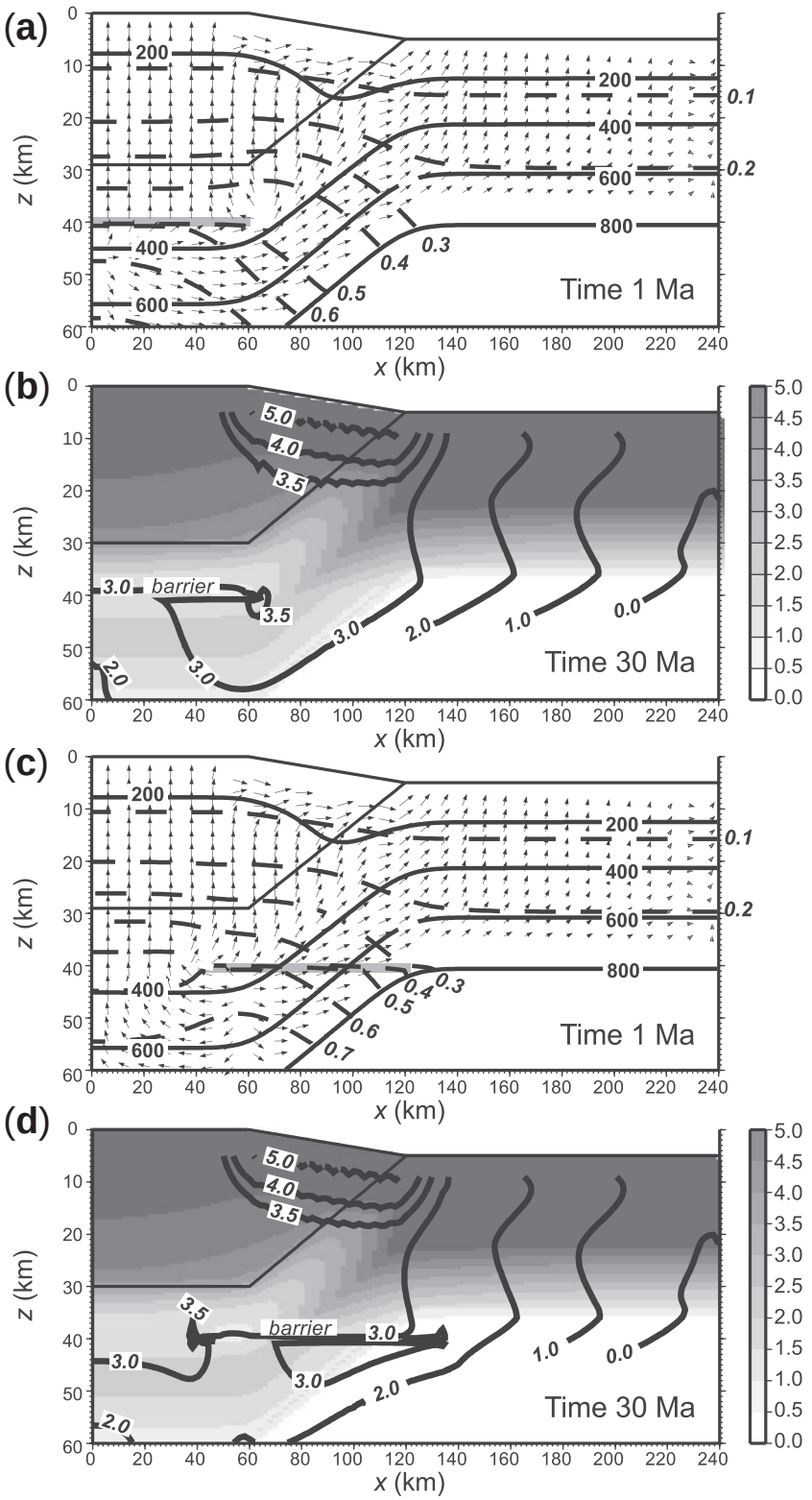

Fig. 7. Model results for cases with barriers to fluid flow, no exhumation. (a) Barrier in the center of the thrust zone (shaded); fluid mass flux after 1 Myr. (b) Bound water content in constituent minerals of the rocks (wt %, shading) and integrated volume fluid fluxes, in $\log_{10} m^3/m^2$ (lines) for the model in (a) after 30 Myr. (c) Barrier to the side of the thrust zone (shaded); fluid mass flux after 1 Myr. (d) Bound water content in rock minerals (wt %, shading) and integrated volume fluid fluxes, in $\log_{10} m^3/m^2$ (lines) for the model in (c) after 30 Myr.

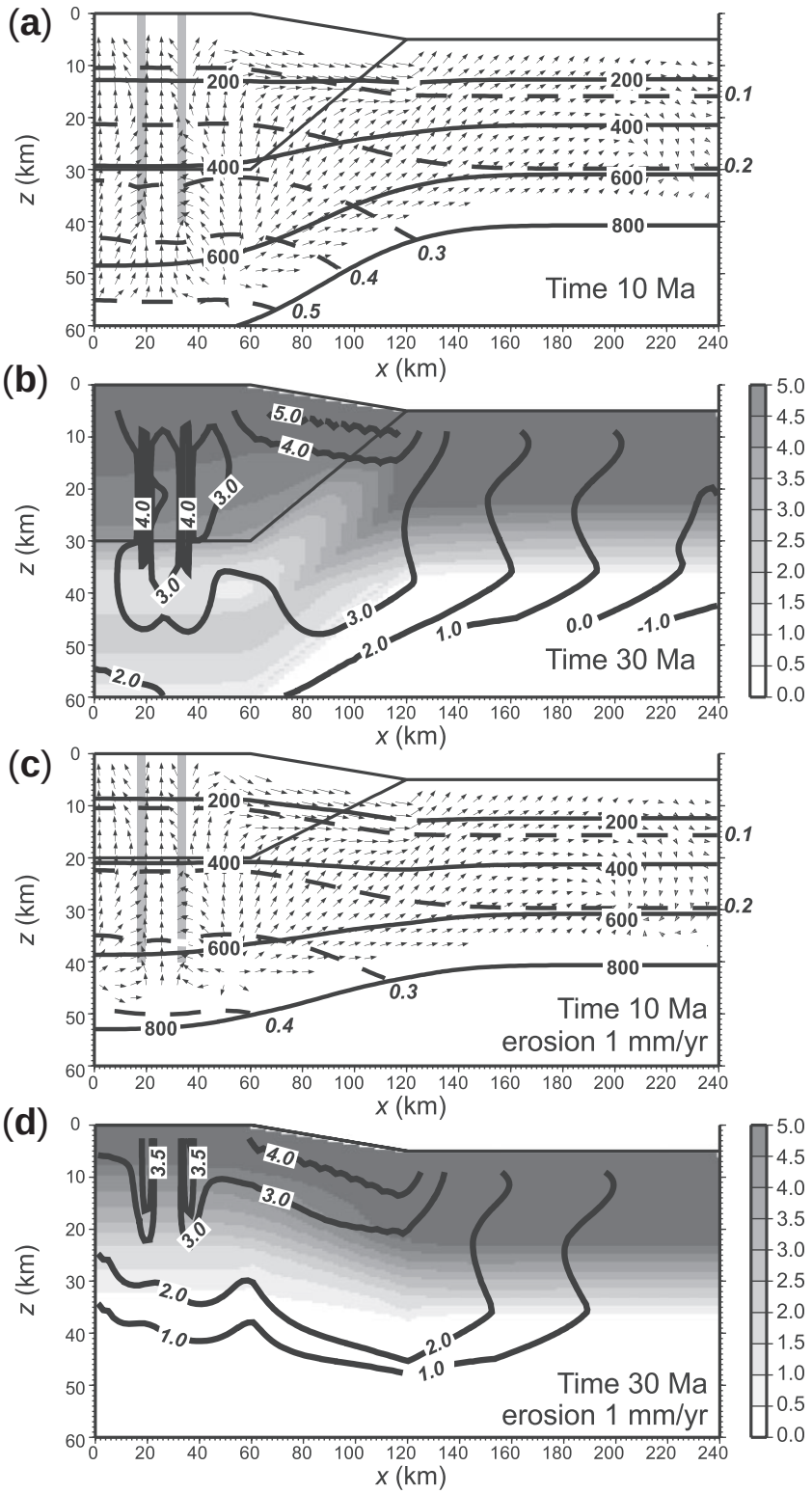

Fig. 8. Model results for cases with permeable channels, background permeability $k_\phi = 10^{-19}$, channel permeability $k_{\phi x} = 10^{-17}$ (horizontal), $k_{\phi z} = 10^{-19}$ (vertical). (a) No exhumation; fluid mass flux after 10 Myr. (b) Bound water content constituent minerals of the rocks (wt %, shading) and integrated volume fluid fluxes, in $\log_{10} m^3/m^2$ (lines) for the model in (a) after 30 Myr. (c) Exhumation rate 1 mm/yr; fluid mass flux after 10 Myr. (d) Bound water content in constituent minerals of the rocks (wt %, shading) and integrated volume fluid fluxes, in $\log_{10} m^3/m^2$ (lines) for the model in (c), after 30 Myr.

products is typically smaller than that of the reactants. Retrograde metamorphism, on the contrary, will lead to clogging of the pore space by the hydration products and to corresponding decreases in permeability. This clogging may slow down and eventually terminate the reaction before the hydration process is completed.

Figure 9a and b illustrates the permeability structure developed in a model incorporating the volume change of metamorphic reaction. The two major hydration zones, in the core and at the side of the thrust, attain the lowest crustal permeability of $10^{-21}\,m^2$ by 1 Ma. Permeability is considerably increased in the dehydrating region wedged between the two low-permeability zones, which results in strong focusing of the fluid flow in this area. In the central part of the thrust, where the dehydration reactions proceed most rapidly, permeability reaches the maximum deep crustal level of $10^{-18}\,m^2$ by 1 Ma. By 12 Ma, most of the lower plate in the thrust zone has a permeability of $10^{-18}\,m^2$ as a result of dehydration (Fig. 9b). The extent of the low-permeability zone in the thrust core diminishes with time and vanishes as cooling in this area is replaced by heating and dehydration reactions start to produce porosity. The low-permeability zone in the center of the model is preserved until the end of the simulation, as no significant dehydration occurs in this area. By 30 Ma, all of the left part of the model has a permeability of $10^{-18}\,m^2$ as a result of continuous dehydration.

When exhumation operates, the development of the permeability contrasts is similar to the case without erosion in the first 10 Myr of the simulation. At later times, rocks that are brought into the shallower parts of the crust by exhumation undergo cooling and hydration. A low-permeability zone develops in the central part of the thrust zone (compare Fig. 9b and 9c). This zone gradually expands with time as more rocks undergo retrograde reactions, thus forming a barrier to fluid flow. The fluid underneath the barrier may occasionally become overpressured and cause the destruction of the low permeability through hydrofracturing. If retrograde reactions are allowed to continue, a low-permeability zone will be developed again.

The temperature distribution in this model is very close to that in a model with homogeneous permeability (Figs 3a, b and 4a). The differences arise mainly in the areas of hydration, where reaction stops as soon as the permeability reaches the lowest permitted value ($10^{-21}\,m^2$). The absence of reaction leads to faster temperature relaxation in these areas. The fluid pressures are similar to those in a homogeneous model, with slight undulations in isobars reflecting focusing of the fluid flow. The time-integrated fluid fluxes also reflect the focusing of the flow in the vicinity of the fault zone (Fig. 9d). The integrated fluxes in the center of the thrust are considerably less than those in a model with homogeneous permeability as a result of the reaction-produced decrease in permeability.

DISCUSSION AND CONCLUSIONS

Our results suggest that a typical fluid flow pattern in an overthrust terrane with the geometry and model parameters explored in this work is upwards in the deep crust below ~20 km for background crustal permeability values $\leq 10^{-19}\,m^2$. The flow is mostly driven by the influx of fluid from metamorphic dehydration at depth. At higher permeability and lower fluid production rates, the metamorphic flux may be surpassed by that produced by thermally induced deviations in fluid density (buoyancy flux). In the presence of lateral temperature gradients, the buoyancy flux will tend to migrate sideways in the direction of decreasing temperature, or in a circular pattern. Such a scenario, however, is unlikely for mid- and lower-crustal conditions, where the plausible permeability values are of the order of $10^{-19}\,m^2$. These results are consistent with the conclusions of Hanson (1992, 1997). Our models, however, are unique in their consideration of the effect of hydration reactions on the 2-D pattern of fluid flow. The consumption of fluid in hydration reactions may lead to transient flow to areas of elevated and gradually decreasing temperature. In particular, downward fluid infiltration may occur at the flanks and within the gradually cooling mid-crustal layers of metamorphic terranes. Such hydration-induced fluxes are small and are likely to occur in areas of low permeability ($\leq 10^{-19}\,m^2$), away from zones of intensive dehydration. Downward flow of fluid may also develop in the central part of the model orogen as a result of rapid cooling and hydration of deep rocks that were brought to shallower parts of the crust during exhumation. These results are consistent with recent field observations suggesting that hydration reactions are responsible for downward fluid flow in the crystalline basement in the Trans-Caucasus region (Yakovlev, 1993) and Central Europe (Stober & Bucher, 2004). The near-hydrostatic fluid pressures observed in deep boreholes, including the 12 km deep well in the Kola Peninsula (Kozlovsky, 1987), may facilitate downward flow to considerable depths.

Low-permeability layers, or barriers, within the deep crust tend to divert fluid from the general upwards motion, and lead to sideways flow. The scale of such flow is determined by the lateral dimensions of the low-permeability layer; in the vicinity of its edges the flow becomes strongly focused in the upward direction. Transient downward flow may occur below the barrier in the presence of strong fluid sources, but fluid circulation does not occur at the values of deep crustal permeability thought plausible ($\sim 10^{-19}\,m^2$).

Our results suggest that up-temperature flow of fluid during orogenic collision in the absence of magmatism is likely to be a transient phenomenon. The major zone of up-temperature flow in our simulations develops during the first 1–3 Myr, in the retrograde area beneath the core of the thrust. During this period the crustal geotherm is

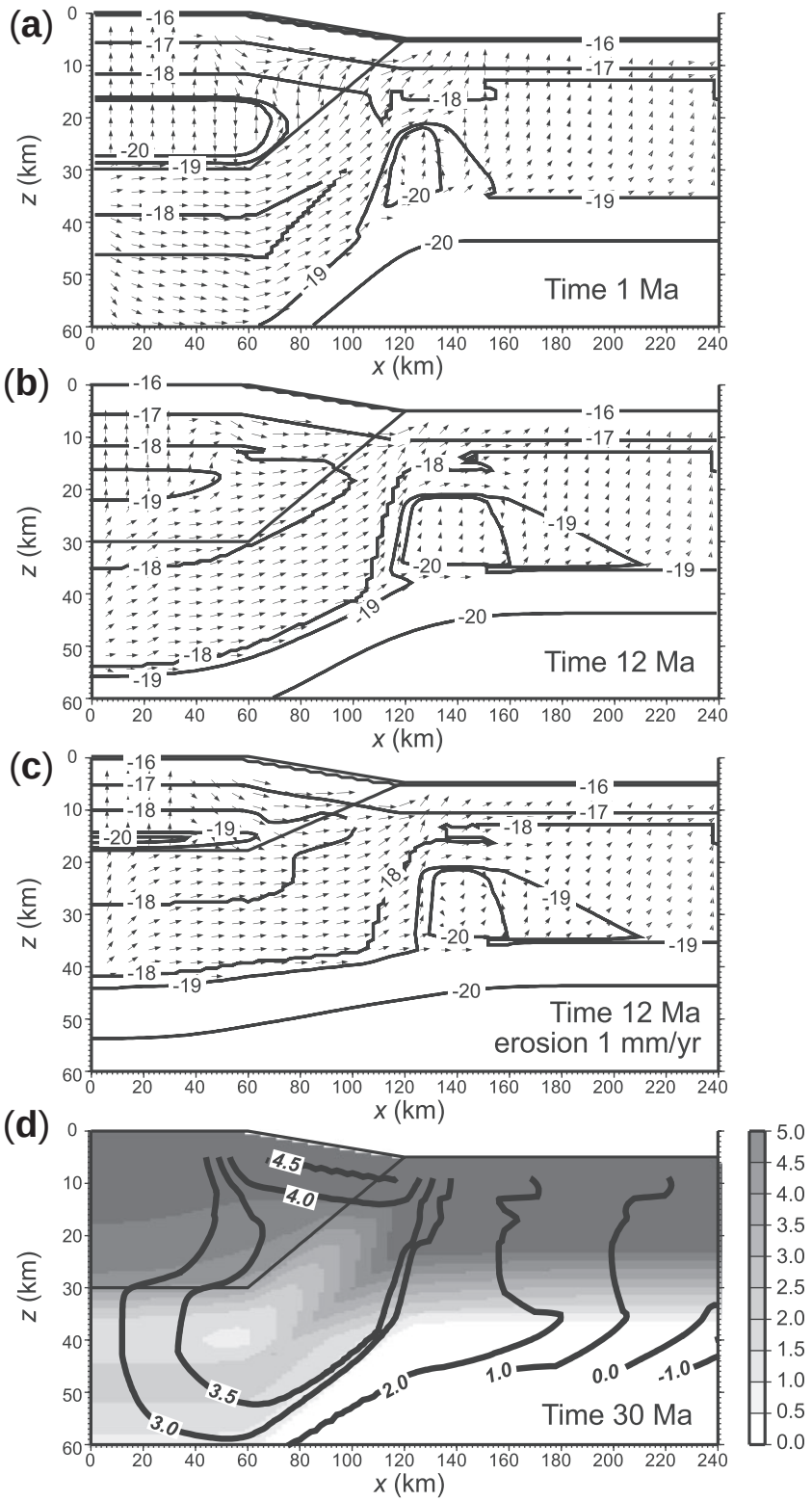

Fig. 9. Model results for the case with permeability evolution produced by metamorphic reactions. (a) No exhumation; fluid mass flux after 1 Myr. Maximum fluid flux below 20 km is within the high-permeability zone, ~0·8 kg/m^2/yr. Lines denote permeability contours, $\log_{10}$ m^2. (b) Same as (a), after 12 Myr. Maximum fluid flux below 20 km is within the high-permeability zone, ~0·25 kg/m^2/yr. (c) Exhumation rate 1 mm/yr; fluid mass flux after 12 Myr. Maximum fluid flux below 20 km is ~0·12 kg/m^2/yr. Lines denote permeability contours, $\log_{10}$ m^2. (d) Bound water content in constituent minerals of the rocks (wt %, shading) and integrated volume fluid fluxes, in $\log_{10}$ m^3/m^2 (lines) for the model in parts (a) and (b) after 30 Myr.

inverted, and the upward flow of fluid in the depth interval 23–30 km is in the direction of increasing temperature. The time-integrated fluxes in this area may exceed 100 m^3/m^2 over 2 Myr. After 3 Myr, however, the inverted geotherm is eliminated and the upward flow of fluid at these depths is down-temperature. Other areas of up-temperature flow are mainly associated with hydration reactions. The zones of hydration in the flanks of the model thrust are relatively long-lived, but the rate of reaction and the fluid fluxes in these areas are extremely small ($\sim$10 m^3/m^2 over 30 Myr). More intensive hydration and the accompanying downward, up-temperature fluid flow may develop during the late stages of exhumation of metamorphic terranes. The size of the flux, however, will depend on the availability of free fluid in the shallower parts of the crust and on the porosity–permeability structure of the metamorphosed rocks. As suggested by some studies (e.g. Balashov & Yardley, 1998), hydration reactions may terminate early as a result of porosity clogging by hydrous minerals.

We note that the up-temperature flow suggested by some studies (e.g. Wing & Ferry, 2002, 2007) coincides with areas of syn-metamorphic plutonism. Although the models presented here (as well as previous models of regional fluid flow; e.g. Hanson, 1997) do not include magmatism, our results suggest that local up-temperature flow may develop in the vicinity of magmatic intrusions as a result of intensive hydration reactions, if strong devolatilization fluxes are absent and if the rock permeability is $\leq 10^{-18}$ m^2. Alternatively, if magmatic intrusions produce an inverted geotherm, the upward flow of fluid from below will be in the direction of increasing temperature.

The temperature evolution of the model crustal section is affected by metamorphic reactions, as in previous models that considered the heat of metamorphic reactions in the overthrust heat budget (e.g. Connolly & Thompson, 1989; Gerya *et al.*, 2002). In Fig. 10a–d, we compare the contributions to the total rock heat budget of all the factors that may influence the temperature evolution of the model terrane: thermal conduction, radiogenic heat production, metamorphic reaction, fluid advection, and erosion. In some cases, the contribution of metamorphic reactions to the total heat budget surpasses those from radiogenic heating or rock advection in the first million years of the thrust history (Fig. 10a and c). By 3 Ma, the amount of heat that is consumed (at the depth 25 km) or released (at the depth 45 km) by metamorphic reactions is equivalent to the heat required to change the temperature of a rock by at least 30–35°C. Field data indicate that our results may in fact be a conservative estimate of the effect of reaction on thermal evolution. The measurements of reaction progress in metacarbonate rock samples made by Ferry (1983) suggest that out of a total heat budget of $\sim 1{\cdot}25 \times 10^9$ J/m^3, $0{\cdot}94 \times 10^9$ J/m^3 rock were converted to chemical work; this amount of heat would raise the temperature of an unreactive rock by $\sim$290°C. In the parameter space of our models, the extraction of 5 wt % of water from a rock with density 2800 kg/m^3 leads to only $\sim 0{\cdot}39 \times 10^9$ J/m^3 of heat that may be released or consumed in metamorphic reactions. The higher values for the heat of reaction derived by Ferry (1983) are partly the result of his study of a metamorphic sequence that underwent infiltration-type reactions involving both CO_2 and water.

The highest model time-integrated fluid fluxes, exceeding 10^4 m^3/m^2, are attained in the upper crust above 15 km depth, underneath the topographic slope. The upper 20 km of the crust below the slope is the zone of mixing of the shallow topography-induced flow and the deep crustal flow produced by metamorphic dehydration, and may be associated with ore-deposition on the flanks of collisional orogens. The time-integrated fluid fluxes in the deep crust below 20 km depth in all of our models are typically of the order of $(1–3) \times 10^3$ m^3/m^2 over 30 Myr, consistent with the estimates of time-integrated fluid fluxes required to account for the progress of mineral reactions as a result of pervasive flow (e.g. Ferry, 1994; Ague, 2003; Wing & Ferry, 2007). As much as 70% of the model fluxes are generated in early times, within 1–3 Myr of the thrust history (Fig. 11). Higher fluxes of $\sim 10^4$ m^3/m^2 may be produced within highly permeable channels. These fluxes are sufficient to cause considerable chemical and isotopic alteration of rocks, consistent with that commonly observed in veined metamorphic systems (e.g. Ague, 1994; Penniston-Dorland & Ferry, 2008). However, the effect of fluid advection on temperature is not large even in these environments. In Fig. 10b and d we compare the contributions to the total heat budget of different components of heat transfer for a model with two permeable channels 2·0 km wide located at 17–18 and 33–34 km in the x direction, with a vertical component of permeability 10^2 times above the background value. The major impact of fluid advection on the total heat budget is in the first few million years, when fluid fluxes are highest as a result of fast rates of metamorphic dehydration. By 1 Ma, the integrated fluxes within the channels already exceed 10^3 m^3/m^2. Nevertheless, even at the top of the entire devolatilization interval, at 30 km depth, the amount of heat transferred by advecting fluid over 3 Myr is equivalent to only about 15°C of temperature change in a rock (Fig. 11). This suggests that the fluid 'hot-spot' environment proposed by Chamberlain & Rumble (1988) requires much faster fluid production rates and larger supplies of water than those used in our modeling. In addition, the advective heat transfer may become more significant as a result of magmatism and associated fluid production, as suggested by Ague & Baxter (2007) for the Barrovian metamorphic terrane in Scotland.

The major difficulty that arises with the modeling presented here, as well as with most other models of fluid

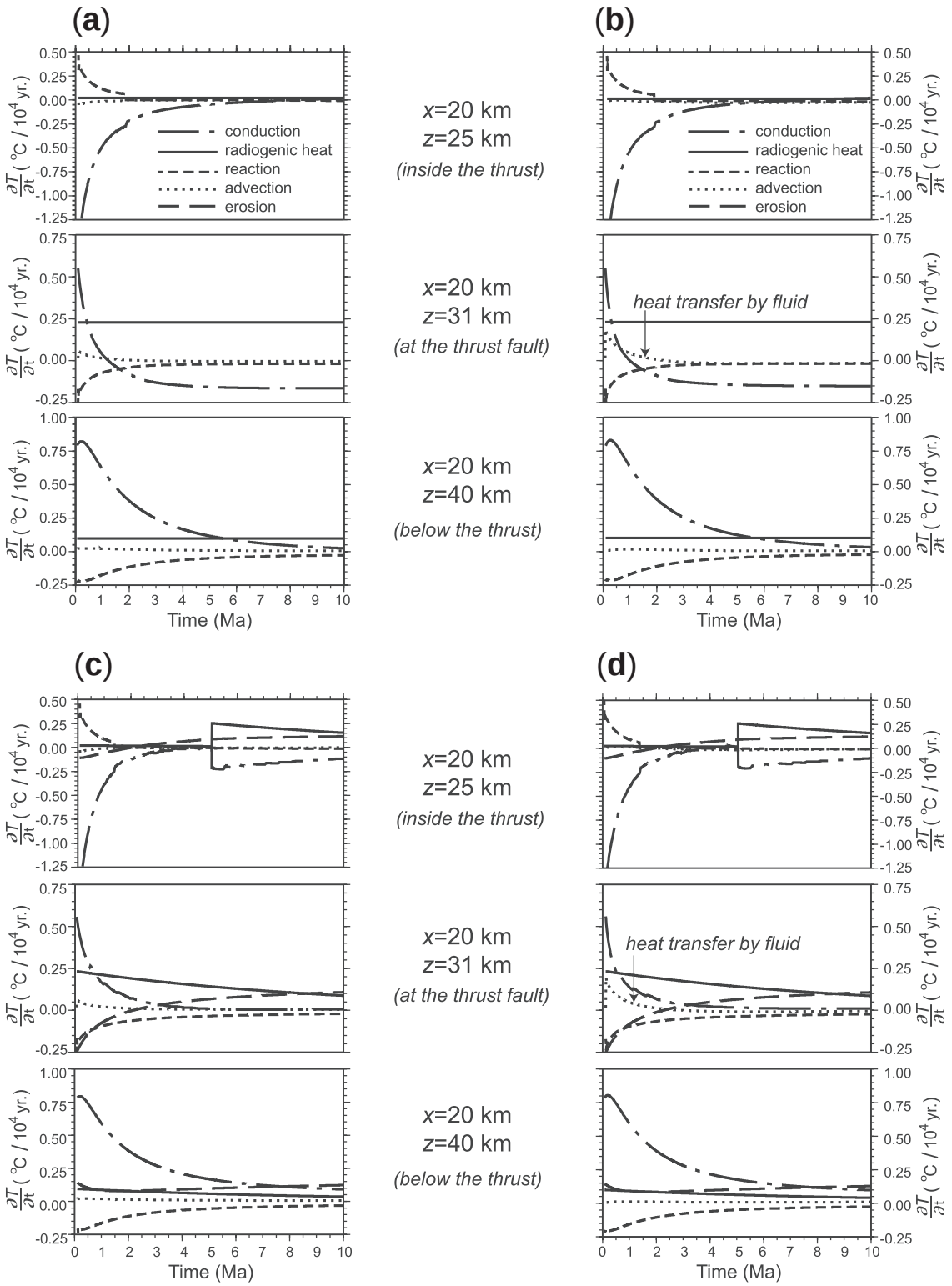

Fig. 10. Contributions of different heat transfer agents (conduction, radiogenic heating, metamorphic reaction, fluid advection, exhumation) to the total temperature change over the first 10 Myr of the model orogen evolution, at different locations within the orogen (in a fixed grid). (a) Model with homogeneous permeability $k_\phi = 10^{-19}$, no exhumation. (b) Model with two permeable channels as in Fig. 8a, no exhumation. (c) Same as (a), with exhumation rate 1 mm/yr. (d) Same as (b), with exhumation rate 1 mm/yr.

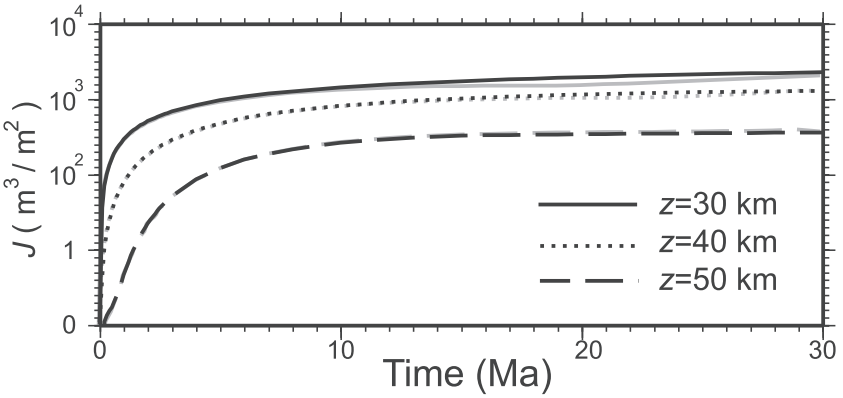

Fig. 11. Time-integrated volume fluid flux as a function of time at different locations within the orogen ($x = 20$ km, $z = 30$, 40, 50 km). Black lines: no exhumation. Grey lines: exhumation rate 1 mm/yr; fluid fluxes are for moving rock parcels (final depth of rocks initially at 30, 40 and 50 km are correspondingly 0, 10 and 20 km).

flow during regional metamorphism, is related to generating near-lithostatic fluid pressures in the deep crust. In all of these models, the rock is assumed to have sufficient strength to maintain networks of connected pores in the entire crustal section. In the absence of fluid sources, the fluid pressure in such systems will always remain near hydrostatic levels. Higher fluid pressures may be achieved only by introducing strong fluid influx from additional sources, such as metamorphic dehydration reactions. The resulting increases in fluid pressure are mainly controlled by the porosity–permeability structure and the rates of fluid influx. At high permeability, extreme and perhaps unrealistically fast rates of fluid production are needed to elevate fluid pressure above the hydrostat. If permeability is low, relatively slow rates of fluid production may result in overpressure, and require the release of fluid by local increases in porosity and permeability. As soon as fluid production ceases, fluid pressures will return to hydrostatic levels regardless of the permeability value.

In reality, such a situation is characteristic for upper crustal conditions, where the rocks are relatively cool and brittle, the porosity is interconnected, and the fluid is generally under hydrostatic pressure. In the middle and lower crust, rocks are thought to behave plastically in response to deformation, with brittle failure occurring only in response to high strain rates such as those during earthquakes or hydrofracturing. Porosity and permeability are likely to be dynamic parameters that evolve in response to the interactions between the deformable solid matrix and the fluid that fills the pores at, or close to, lithostatic pressure. A more suitable description of lower crustal conditions, therefore, should include an explicit treatment of the plastic behavior of rocks, and the physical interactions between the fluid and the deformable rock matrix (e.g. Connolly & Podladchikov, 1998; Vasilyev *et al.*, 1998; Lyubetskaya & Ague, 2007).

The model limitations, however, are unlikely to affect our major conclusions regarding the large-scale behavior of fluid flow at plausible values of crustal permeability ($\sim 10^{-19}$ m^2). Plastic deformation such as pore compaction may perhaps facilitate the upward flow of fluid released by dehydration reactions in the middle and deep crust, but is not expected to significantly divert flow from the general sub-vertical direction. In fact, the interconnected porosity and the absence of rock deformation in our models form the most favorable environment for circular and downward flow of fluid. The limited occurrence of such flow patterns in our models suggests that the upward and down-temperature flow of fluid should dominate at deep-crustal conditions in the absence of magmatism and barriers to flow. Nevertheless, the observation of transient up-temperature flow driven by hydration reactions in certain geological settings indicates that this phenomenon may occur despite deformation-produced changes in permeability and porosity at least at some stages of orogen history.

ACKNOWLEDGEMENTS

We gratefully acknowledge the helpful review comments of K. A. Evans, T. Gerya and S. Penniston-Dorland, and the support of the National Science Foundation Directorate for Geosciences (NSF EAR-0509934).

REFERENCES

Ague, J. J. (1994). Mass transfer during Barrovian metamorphism of pelites, south–central Connecticut: II. Channelized fluid flow and the growth of staurolite and kyanite. *American Journal of Science* **294**, 1061–1134.

Ague, J. J. (2003). Fluid flow in the deep crust. In: Holland, H. & Turekian, K.K. (eds.) *Treatise on Geochemistry* **3**, Amsterdam, Elsevier, 195–228.

Ague, J. J. & Baxter, E. F. (2007). Brief thermal pulses during mountain building recorded by Sr diffusion in apatite and multicomponent in garnet. *Earth and Planetary Science Letters* **261**, 500–516.

Ague, J. J. & Rye, D. M. (1999). Simple models of CO_2 release from metacarbonates with implications for interpretation of direction

and magnitude of fluid flow in the deep crust. *Journal of Petrology* **40**, 1443–1462.

Balashov, V. N. & Yardley, B. W. D. (1998). Modeling metamorphic fluid flow with reaction–compaction–permeability feedbacks. *American Journal of Science* **298**, 441–470.

Baumgartner, L. P. & Ferry, J. M. (1991). A model for coupled fluid-flow and mixed-volatile mineral reactions with applications to regional metamorphism. *Contributions to Mineralogy and Petrology* **106**, 273–285.

Brace, W. F. (1980). Permeability of crystalline and argillaceous rocks. *International Journal of Rock Mechanics and Mining Sciences* **17**, 241–251.

Brady, J. B. (1988). The role of volatiles in the thermal history of metamorphic terranes. *Journal of Petrology* **29**, 1187–1213.

Bredehoeft, J. D. & Hanshaw, B. B. (1968). On the maintenance of anomalous fluid pressures: I. Thick sedimentary sequences. *Geological Society of America Bulletin* **79**, 1097–1106.

Breeding, C. M. & Ague, J. J. (2002). Slab-derived fluids and quartz-vein formation in an accretionary prism, Otago Schist, New Zealand. *Geology* **30**, 499–502.

Cermak, V. (1993). Lithospheric thermal regimes in Europe. *Physics of the Earth and Planetary Interiors* **79**, 179–193.

Chamberlain, C. P. & Rumble, D. (1988). Thermal anomalies in a regional metamorphic terrane: An isotopic study of the role of fluids. *Journal of Petrology* **29**, 1215–1232.

Chamberlain, C. P. & Rumble, D. (1989). The influence of fluids on the thermal history of a metamorphic terrain: New Hampshire, USA. In: Daly, J. S., Cliff, R. A. & Yardley, B. W. D. (eds.) *Evolution of Metamorphic Belts. Geological Society, London, Special Publications* **43**, 203–213.

Connolly, J. A. D. (1997). Devolatilization-generated fluid pressure and deformation-propagated fluid flow during prograde regional metamorphism. *Journal of Geophysical Research* **102**, 18149–18173.

Connolly, J. A. D. & Podladchikov, Y. Y. (1998). Compaction-driven fluid flow in viscoelastic rock. *Geodinamica Acta* **11**, 55–84.

Connolly, J. A. D. & Podladchikov, Y. Y. (2000). Temperature-dependent viscoelastic compaction and compartmentalization in sedimentary basins. *Tectonophysics* **324**, 137–168.

Connolly, J. A. D. & Thompson, A. B. (1989). Fluid and enthalpy production during regional metamorphism. *Contributions to Mineralogy and Petrology* **102**, 347–366.

Cui, X., Nabelek, P. I. & Liu, M. (2002). Numerical modeling of fluid flow and oxygen isotope exchange in the Notch Peak contact-metamorphic aureole, Utah. *Geological Society of America Bulletin* **114**, 869–882.

David, C., Wong, T.-F., Zhu, W. & Zhang, J. (1994). Laboratory measurement of compaction-induced permeability change in porous rocks: Implications for the generation and maintenance of pore pressure excess in the crust. *Pure and Applied Geophysics* **143**, 425–456.

Dipple, G. M. & Ferry, J. M. (1992). Fluid flow and stable isotopic alteration in rocks at elevated temperatures with applications to metamorphism. *Geochimica et Cosmochimica Acta* **56**, 3539–3550.

England, P. C. & Thompson, A. B. (1984). Pressure–temperature–time paths of regional metamorphism. 1. Heat transfer during the evolution of regions of thickened continental crust. *Journal of Petrology* **25**, 894–928.

Etheridge, M. A., Wall, V. J. & Vernon, R. H. (1983). The role of fluid phase during regional metamorphism and deformation. *Journal of Metamorphic Geology* **1**, 205–226.

Etheridge, M. A., Wall, V. J., Cox, S. F. & Vernon, R. H. (1984). High fluid pressures during regional metamorphism and deformations: Implications for mass transport and deformations mechanisms. *Journal of Geophysical Research* **89**, 4344–4358.

Evans, K. A. & Bickle, M. J. (1999). Determination of time-integrated metamorphic fluid fluxes from the reaction progress of multivariant assemblages. *Contributions to Mineralogy and Petrology* **134**, 277–293.

Ferry, J. M. (1983). On the control of temperature, fluid composition, and reaction progress during metamorphism. *American Journal of Science* **283**, 201–232.

Ferry, J. M. (1992). Regional metamorphism of the Waits River Formation, eastern Vermont: delineation of a new type of giant metamorphic hydrothermal system. *Journal of Petrology* **33**, 45–94.

Ferry, J. M. (1994). Overview of the petrologic record of fluid flow during regional metamorphism in Northern New England. *American Journal of Science* **294**, 905–988.

Forster, C. B. & Evans, J. P. (1991). Hydrogeology of thrust faults and crystalline thrust sheets: Results of combined field and modeling studies. *Geophysical Research Letters* **18**, 979–982.

Garven, G. (1995). Continental-scale groundwater flow and geologic processes. *Annual Review of Earth and Planetary Sciences* **23**, 89–117.

Garven, G. & Freeze, R. A. (1984*a*). Theoretical analysis of the role of groundwater flow in the genesis of stratabound ore deposits: 1. Mathematical and numerical model. *American Journal of Science* **284**, 1085–1124.

Garven, G. & Freeze, R. A. (1984*b*). Theoretical analysis of the role of groundwater flow in the genesis of stratabound ore deposits: 1. Quantitative results. *American Journal of Science* **284**, 1125–1174.

Gerya, T. V., Perchuk, L. L., Maresch, W. V., Willner, A. P., Van Reenen, D. D. & Smit, C. A. (2002). Thermal regime and gravitational instability of multi-layered continental crust: implications for the buoyant exhumation of high-grade metamorphic rocks. *European Journal of Mineralogy* **14**, 687–699.

Hanson, R. B. (1992). Effects of fluid production on fluid flow during regional and contact metamorphism. *Journal of Metamorphic Geology* **10**, 87–97.

Hanson, R. B. (1995). Hydrodynamics of contact metamorphism. *Geological Society of America Bulletin* **108**, 1594–1607.

Hanson, R. B. (1997). Hydrodynamics of regional metamorphism due to continental collision. *Economic Geology* **92**, 880–891.

Hanson, R. B. & Barton, M. D. (1989). Thermal development of low-pressure metamorphic belts: Results from two-dimensional numerical models. *Journal of Geophysical Research* **94**, 10363–10377.

Holland, T. & Powell, R. (1991). A Compensated-Redlich–Kwong (CORK) equation for volumes and fugacities of CO_2 and H_2O in the range 1 bar to 50 kbar and 100–1600°C. *Contributions to Mineralogy and Petrology* **109**, 265–273.

Holland, T. & Powell, R. (1998). An internally consistent thermodynamic data set for phases of petrological interest. *Journal of Metamorphic Geology* **16**, 309–343.

Ingebritsen, S. E. & Manning, C. E. (1999). Geological implications of a permeability depth curve for the continental crust. *Geology* **27**, 1107–1110.

Jamieson, R. A., Beaumont, C., Fullsack, P. & Lee, B. (1998). Barrovian regional metamorphism: where's the heat? In: Treolar, P. J. & O'Brien, P. J. (eds.) *What Drives Metamorphism and Metamorphic Reactions?* **138**, 23–51, Geological Society, London, Special publications.

Jaupart, C. & Mareschal, J.-C. (2003). Constraints on crustal heat production from heat flow data. In: Holland, H. & Turekian, K. K. (eds.) *Treatise On Geochemistry* **3**, Amsterdam, Elsevier, 65–84.

Koons, P. O. & Craw, D. (1991). Evolution of fluid driving forces and composition within collisional orogens. *Geophysical Research Letters* **18**, 935–938.

Kozlovsky, Y. A. (1987). *The Superdeep Well of the Kola Peninsula*. New York Springer.

Luttge, A., Bolton, E. W. & Rye, D. M. (2004). A kinetic model of metamorphism: an application to siliceous dolomites. *Contributions to Mineralogy and Petrology* **146**, 546–565.

Lyubetskaya, T. & Ague, J. J. (2007). New models of crustal fluid flow incorporating magmatism and porosity evolution during orogenesis. *EOS Transactions, American Geophysical Union* **88**(52), Fall Meeting Supplement Abstracts V23A–1233.

Manning, C. E. & Ingebritsen, S. E. (1999). Permeability of the continental crust: implications of geothermal data and metamorphic systems. *Reviews of Geophysics* **37**, 127–150.

Miller, S. A., van der Zee, W., Olgaard, D. L. & Connolly, J. A. D. (2003). A fluid-pressure feedback model of dehydration reactions: experiments, modelling, and application to subduction zones. *Tectonophysics* **370**, 241–251.

Morency, C., Huismans, R. S., Beaumont, C. & Fullsack, P. (2007). A numerical model for coupled fluid flow and matrix deformation with applications to disequilibrium compaction and delta stability. *Journal of Geophysical Research* **112**, B10407, doi:10.1029/2006JB004701.

Oliver, N. H. S. (1996). Review and classification of structural controls on fluid flow during regional metamorphism. *Journal of Metamorphic Geology* **17**, 477–492.

Peacock, S. M. (1987). Thermal effects of metamorphic fluids in subduction zones. *Geology* **15**, 1057–1060.

Peacock, S. M. (1989). Numerical constraints on rates of metamorphism, fluid production, and fluid flux during regional metamorphism. *Geological Society of America Bulletin* **101**, 476–485.

Penniston-Dorland, S. C. & Ferry, J. M. (2008). Element mobility and scale of mass transport in the formation of quartz veins during regional metamorphism of the Waits River Formation, east-central Vermont. *American Mineralogist* **93**, 7–21.

Pollack, H. N., Hurter, S. J. & Johnson, J. R. (1993). Heat flow from the Earth's interior: Analysis of the global data set. *Reviews of Geophysics* **31**, 267–280.

Ramsay, J. G. (1980). The crack-seal mechanism of rock deformation. *Nature* **284**, 135–139.

Ridley, J. (1986). Modelling of the relations between reaction enthalpy and the buffering of reaction progress in metamorphism. *Mineralogical Magazine* **50**, 375–384.

Rimi, A. (1999). Mantle heat flow and geotherms for the main geologic domains in Morocco. *International Journal of Earth Sciences* **88**, 458–466.

Rudnick, R. L. & Fountain, D. M. (1995). Nature and composition of the continental crust: a lower crustal perspective. *Reviews of Geophysics* **33**, 267–309.

Rudnick, R. L., McDonough, W. F. & O'Connell, R. J. (1998). Thermal structure, thickness and composition of continental lithosphere. *Chemical Geology* **145**, 395–411.

Rumble, D. & Spear, F. S. (1983). Oxygen isotope equilibration and permeability enhancement during regional metamorphism. *Journal of the Geological Society, London* **140**, 619–628.

Sclater, J. G., Parsons, B. & Jaupart, C. (1981). Oceans and continents: similarities and differences in the mechanisms of heat loss. *Journal of Geophysical Research* **86**, 11535–11552.

Shi, Y. & Wang, C.-Y. (1987). Two-dimensional modeling of the P–T–t paths of regional metamorphism in simple overthrust terrains. *Geology* **15**, 1048–1051.

Skelton, A. D. L. (1996). The timing and direction of metamorphic fluid flow in Vermont. *Contributions to Mineralogy and Petrology* **125**, 75–84.

Sleep, N. H. & Blanpied, M. L. (1992). Creep, compaction and the weak rheology of major faults. *Nature* **259**, 687–692.

Stober, I. & Bucher, K. (2004). Fluid sinks within the Earth's crust. *Geofluids* **4**, 143–151.

Suetnova, E. & Vasseur, G. (2000). 1-D modelling rock compaction in sedimentary basins using visco-elastic rheology. *Earth and Planetary Science Letters* **178**, 373–383.

Tenthorey, E. & Cox, S. F. (2003). Reaction-enhanced permeability during serpentinite dehydration. *Geology* **31**, 921–924.

Turcotte, D. L. & Schbert, G. (2002). *Geodynamics: Applications of Continuum Physics to Geological Problems*. New York: John Wiley, 456 pp.

Vasilyev, O. V., Podladchikov, Y. Y. & Yuen, D. A. (1998). Modeling of compaction driven flow in poro-viscoelastic medium using adaptive wavelet collocation method. *Geophysical Research Letters* **25**, 3239–3242.

Walder, J. & Nur, A. (1984). Porosity reduction and crustal pore pressure development. *Journal of Geophysical Research* **89**, 11539–11548.

Walther, J. V. & Orville, P. M. (1982). Volatile production and transport during metamorphism. *Contributions to Mineralogy and Petrology* **79**, 252–257.

Wing, B. A. & Ferry, J. M. (2002). Three-dimensional geometry of metamorphic fluid flow during Barrovian regional metamorphism from an inversion of combined petrologic and stable isotope data. *Geology* **30**, 639–642.

Wing, B. A. & Ferry, J. M. (2007). Magnitude and geometry of reactive fluid flow from direct inversions of spatial patterns of geochemical alteration. *American Journal of Science* **307**, 793–832.

Wong, T.-F. & Zhu, W. (1999). Brittle faulting and permeability evolution: hydromechanical measurement, microstructural observation, and network modeling. In: *Faults and Subsurface Fluid Flow in the Shallow Crust* **113**, Washington, DC: American Geophysical Union 83–99.

Yakovlev, L. Y. (1993). The role of metamorphism of the basaltic basement of sedimentary basins in crustal evolution. *International Geology Review* **35**, 27–47.

Zhang, S., FitzGerald, J. D. & Cox, S. F. (2000). Reaction-enhanced permeability during decarbonation of calcite + quartz → wollastonite + carbon dioxide. *Geology* **28**, 911–914.

JOURNAL OF PETROLOGY | VOLUME 50 | NUMBER 12 | PAGE 2375 | 2009 | doi:10.1093/petrology/egp100

Erratum

Modeling the Magnitudes and Directions of Regional Metamorphic Fluid Flow in Collisional Orogens

Journal of Petrology 2009, volume 50, pp. 1505–1531.

T. LYUBETSKAYA AND J. J. AGUE

DEPARTMENT OF GEOLOGY AND GEOPHYSICS, YALE UNIVERSITY, PO BOX 208109, NEW HAVEN, CT 06520-8109, USA

The sentence:

By 3 Ma, the amount of heat that is consumed (at the depth 25 km) or released (at the depth 45 km) by metamorphic reactions is equivalent to the heat required to change the temperature of a rock by at least 30–35°C.

On page 1527, column 1, paragraph 3, should read:

By 3 Ma, the amount of heat that is consumed (at the depth 45 km) or released (at the depth 25 km) by metamorphic reactions is equivalent to the heat required to change the temperature of a rock by at least 30–35°C.